Comput Mech (2008) 41:527–545
DOI 10.1007/s00466-007-0209-3

ORIGINAL PAPER

SSPH basis functions for meshless methods, and comparison of solutions with strong and weak formulations

R. C. Batra · G. M. Zhang

Received: 7 February 2007 / Accepted: 7 July 2007 / Published online: 10 August 2007

Abstract We propose a new and simple technique called the Symmetric Smoothed Particle Hydrodynamics (SSPH) method to construct basis functions for meshless methods that use only locations of particles. These basis functions are found to be similar to those in the Finite Element Method (FEM) except that the basis for the derivatives of a function need not be obtained by differentiating those for the function. Of course, the basis for the derivatives of a function can be obtained by differentiating the basis for the function as in the FEM and meshless methods. These basis functions are used to numerically solve two plane stress/strain elasto-static problems by using either the collocation method or a weak formulation of the problem defined over a subregion of the region occupied by the body; the latter is usually called the Meshless Local Petrov–Galerkin (MLPG) method. For the two boundary-value problems studied, it is found that the weak formulation in which the basis for the first order derivatives of the trial solution are derived directly in the SSPH method (i.e., not obtained by differentiating the basis function for the trial solution) gives the least value of the L^2-error norm in the displacements while the collocation method employing the strong formulation of the boundary-value problem has the largest value of the L^2-error norm. The numerical solution using the weak formulation requires more CPU time than the solution with the strong formulation of the problem. We have also computed the L^2-error norm of displacements by varying the number of particles, the number of Gauss points used to numerically evaluate domain integrals appearing in the weak formulation of the problem, the radius of the compact support of the kernel function used to generate the SSPH basis, the order of complete monomials employed for constructing the SSPH basis, and boundary conditions used at a point on a corner of the rectangular problem domain. It is recommended that for solving two-dimensional elasto-static problems, the MLPG formulation in which derivatives of the trial solution are found without differentiating the SSPH basis function be adopted.

Keywords Symmetric smoothed particle hydrodynamics (SSPH) basis · MLPG · Error norm · Strong and weak formulations · Stress concentration

R. C. Batra · G. M. Zhang (✉)
Department of Engineering Science and Mechanics,
Virginia Polytechnic Institute and State University,
Blacksburg, VA 24061, USA
e-mail: gazhang1@vt.edu

1 Introduction

The meshless Smoothed Particle Hydrodynamics (SPH) method, proposed by Lucy [1] to study three-dimensional (3D) astrophysics problems, has been successfully applied to analyze transient fluid and solid mechanics problems. However, it has two shortcomings, namely inaccuracy at particles on the boundary and the tensile instability. Many techniques have been developed to alleviate these two deficiencies, among which are the Corrected Smoothed Particle Method (CSPM) [2,3], the Reproducing Kernel Particle Method (RKPM) [4–6] and the Modified Smoothed Particle Hydrodynamics (MSPH) method [7–10]. The MSPH method has been successfully applied to study wave propagation in functionally graded materials [9], capture the stress field near a crack-tip, and simulate the propagation of multiple cracks [10] in a linear elastic body.

However, the MSPH method requires that all derivatives of the kernel function used to generate values of the trial solution and its derivatives at a point be non-constants, which

restricts the choice of the kernel function. Furthermore, the matrix to be inverted for finding kernel estimates of the trial solution and its derivatives is asymmetric. In [11] we proposed the Symmetric Smoothed Particle Hydrodynamics (SSPH) method which made the matrix to be inverted symmetric, reduced the storage requirement and the CPU time, eliminated the requirement that the kernel function must not be a constant, and more importantly, gave a lower error in the numerical solution than that obtained with the MSPH method. Also requirements on the kernel function used to generate basis functions with the SSPH method were compared with those for the RKPM and the MLS [12] method, and errors in interpolating an exponential function with the three sets of basis functions were computed. The SSPH basis functions together with the collocation method or the strong formulation of the problem were used to solve an elasto-static problem. However, the collocation method requires the computation of 2nd order derivatives for an elastic problem. Said differently, the basis functions must be at least twice differentiable. One can reduce this differentiability requirement by employing a weak formulation of the problem as is done in the Finite Element Method (FEM) and some meshless methods such as the Element Free Galerkin [13] and the Meshless Local Petrov–Galerkin (MLPG) [14]. As far as we can ascertain, the first order derivatives of the trial solution have been computed by differentiating the shape or the basis functions. However, in the SSPH basis functions presented in [11] and further improved upon here, one can find the spatial derivatives of the trial solution without differentiating the basis functions. That is, basis functions for the spatial derivatives are different from those for the trial solution and the former are not derivatives of the latter.

We note that the idea of approximating derivatives of a function without differentiating the basis functions has been introduced by Kim and Liu [15] and Kim et al. [16] for the MLS method, and by Li and Liu [17,18] who used the wavelet functions and developed the hierarchical basis for the meshless method. Similar ideas can also be found in [19,20]. Here we start with the Taylor series expansion of a function as is often done in the SPH method, and address the question of whether or not solving for derivatives of a function without differentiating the basis functions leads to lower errors in the numerical solution of boundary-value problems. For this purpose, we study two elasto-static problems and compare L^2-error norms of displacements computed with three methods, namely the collocation method, and the MLPG method with spatial derivatives of the trial solution obtained with and without differentiating the SSPH basis functions. It is found that indeed the MLPG formulation with spatial derivatives of the trial solution computed without differentiating the SSPH basis functions gives the least value of the L^2-error norm of displacements, and the collocation method has the largest value of this error norm. It is thus concluded that it is better to use the weak form without differentiating the SSPH basis functions to solve elasto-static problems. Since the weak and the strong formulations of an elasto-static problem have, respectively, first and second order derivatives of displacements, one can decrease the order of complete monomials used to construct the SSPH basis functions when using the weak formulation and thereby economize on the CPU time to compensate somewhat for the increase in the CPU time required to numerically evaluate domain integrals. Numerical results show that the weak formulation without differentiating the SSPH basis functions and using complete monomials of degree one still gives a lower value of the L^2-error norms in displacements than the collocation method for which the SSPH basis functions are generated by employing complete monomials of degree two.

Ferreira et al. [21] have analyzed beam and plate problems with the collocation method and the radial basis functions (RBFs) but have not compared approximate solutions computed with the weak and the strong formulations. Qian et al. [22] have compared approximate solutions for higher-order plate theories found with two MLPG formulations first by taking the test function equal to the kernel or the weight function used to generate basis function by the MLS method and then by setting the test function equal to a MLS basis function. They found that the second formulation, which equals the Galerkin formulation of the problem over a subdomain of the body, gives lower errors in the computed displacements and stresses than the first one. Batra et al. [23] have employed the same two MLPG formulations to study axisymmetric transient heat conduction in a bimetallic disk. Xiao and McCarthy [24] have employed a local weak form of the equilibrium equations governing infinitesimal deformations of a linear elastic body, the RBFs, and taken the Heaviside function as the test function. The RBFs possess the Kronecker delta property; therefore no special algorithm is needed to satisfy essential boundary conditions.

The rest of the paper is organized as follows. Section 2 describes the SSPH basis functions. In Sect. 3, the strong and the weak form of equations of equilibrium for a 2D elastic problem are summarized. Numerical results for plane stress deformations of a rectangular plate with essential boundary conditions applied on one edge and natural boundary conditions on the remaining three edges are presented in Sect. 4. The effect of using different number of particles, the integration rule to evaluate domain integrals, and boundary conditions imposed at a particle on a corner of the plate etc. are delineated. Subsequently, the stress concentration near a circular hole in a semi-infinite elastic plate with a hole at the center is analyzed by the three techniques. Conclusions of this work are summarized in Sect. 5.

2 Symmetric smoothed particle hydrodynamics basis functions

For a function $f(\mathbf{x})$ having continuous derivatives up to $(n+1)$th order, the value of the function at a point $\boldsymbol{\xi} = (\xi_1, \xi_2, \xi_3)$ located in the neighborhood of $\mathbf{x} = (x_1, x_2, x_3)$ can be approximated through the finite Taylor series expansion

$$f(\xi_1,\xi_2,\xi_3) = \sum_{m=0}^{n} \frac{1}{m!} \left[(\xi_1 - x_1) \frac{\partial}{\partial x_1} + (\xi_2 - x_2) \frac{\partial}{\partial x_2} + (\xi_3 - x_3) \frac{\partial}{\partial x_3} \right]^m f(x_1, x_2, x_3), \tag{2.1}$$

where the symbol ! denotes factorial with $0! = 1$. Neglecting the third and the higher order terms, and introducing two matrices, $\mathbf{P}(\boldsymbol{\xi}, \mathbf{x})$ and $\mathbf{Q}(\mathbf{x})$ we write Eq. (2.1) as

$$f(\boldsymbol{\xi}) = \mathbf{P}(\boldsymbol{\xi}, \mathbf{x})\, \mathbf{Q}(\mathbf{x}), \tag{2.2}$$

where

$$\mathbf{Q}(\mathbf{x}) = \left[f(\mathbf{x}), \frac{\partial f(\mathbf{x})}{\partial x_1}, \frac{\partial f(\mathbf{x})}{\partial x_2}, \frac{\partial f(\mathbf{x})}{\partial x_3}, \frac{1}{2}\frac{\partial^2 f(\mathbf{x})}{\partial x_1^2}, \frac{1}{2}\frac{\partial^2 f(\mathbf{x})}{\partial x_2^2}, \frac{1}{2}\frac{\partial^2 f(\mathbf{x})}{\partial x_3^2}, \frac{\partial^2 f(\mathbf{x})}{\partial x_1 \partial x_2}, \frac{\partial^2 f(\mathbf{x})}{\partial x_2 \partial x_3}, \frac{\partial^2 f(\mathbf{x})}{\partial x_1 \partial x_3} \right]^T, \tag{2.3}$$

$$\mathbf{P}(\boldsymbol{\xi} - \mathbf{x}) = \left[1, \xi_1 - x_1, \xi_2 - x_2, \xi_3 - x_3, (\xi_1 - x_1)^2, (\xi_2 - x_2)^2, (\xi_3 - x_3)^2, (\xi_1 - x_1)(\xi_2 - x_2), (\xi_2 - x_2)(\xi_3 - x_3), (\xi_1 - x_1)(\xi_3 - x_3) \right].$$

Elements of matrix $\mathbf{Q}(\mathbf{x})$, the kernel estimate of the function, its first derivatives and its second derivatives at $\mathbf{x} = (x_1, x_2, x_3)$ are the unknown variables to be found from Eq. (2.2). As will become clear later, elements of matrix $\mathbf{P}(\boldsymbol{\xi}, \mathbf{x})$ can be associated with shape functions used in the FEM.

In the MSPH method [7], we find the matrix $\mathbf{Q}(\mathbf{x})$ by multiplying both sides of Eq. (2.2) with a positive valued kernel function $W(\boldsymbol{\xi}, \mathbf{x})$ of compact support, the first and the second derivatives of the kernel function, and integrating the resulting equations over the compact support of the kernel function. The matrix so obtained that operates on the matrix $\mathbf{Q}(\mathbf{x})$ is asymmetric and in order for it be non-singular, the first and the second derivatives of the kernel function $W(\boldsymbol{\xi}, \mathbf{x})$ must not be constants. This restricts the choice of the kernel function. In order to be able to use a wider class of kernel functions and have the matrix pre-multiplying the matrix

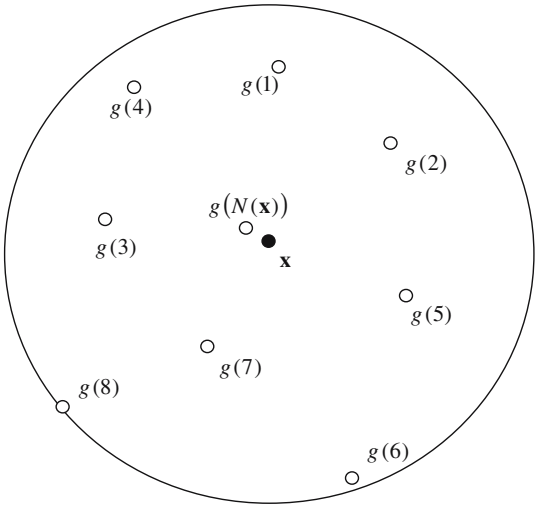

Fig. 1 Distribution of particles in the compact support of the kernel function $W(\boldsymbol{\xi}, \mathbf{x})$ associated with the point $\mathbf{x} = (x_1, x_2, x_3)$

$\mathbf{Q}(\mathbf{x})$ symmetric, we proposed the SSPH method [11]. In it, we multiply both sides of Eq. (2.2) with $W(\boldsymbol{\xi}, \mathbf{x})\, \mathbf{P}(\boldsymbol{\xi}, \mathbf{x})^T$ and obtain

$$\begin{aligned} & f(\boldsymbol{\xi})\, W(\boldsymbol{\xi}, \mathbf{x})\, \mathbf{P}(\boldsymbol{\xi}, \mathbf{x})^T \\ &= \mathbf{P}(\boldsymbol{\xi}, \mathbf{x})\, \mathbf{Q}(\mathbf{x}) W(\boldsymbol{\xi}, \mathbf{x})\, \mathbf{P}(\boldsymbol{\xi}, \mathbf{x})^T, \\ &= \left[\mathbf{P}(\boldsymbol{\xi}, \mathbf{x})^T\, W(\boldsymbol{\xi}, \mathbf{x})\, \mathbf{P}(\boldsymbol{\xi}, \mathbf{x}) \right] \mathbf{Q}(\mathbf{x}). \end{aligned} \tag{2.4}$$

In the compact support of the kernel function $W(\boldsymbol{\xi}, \mathbf{x})$ associated with the point $\mathbf{x} = (x_1, x_2, x_3)$, shown in Fig. 1, let there be $N(\mathbf{x})$ particles. In the global numbering system, let the particle number of the jth particle in the compact support of $W(\boldsymbol{\xi}, \mathbf{x})$ be $g(j)$. We evaluate Eq. (2.4) at every particle in the compact support of $W(\boldsymbol{\xi}, \mathbf{x})$ and sum each side over these particles to arrive at

$$\begin{aligned} & \sum_{j=1}^{N(\mathbf{x})} f\left(\boldsymbol{\xi}^{g(j)}\right) W\left(\boldsymbol{\xi}^{g(j)}, \mathbf{x}\right) \mathbf{P}\left(\boldsymbol{\xi}^{g(j)}, \mathbf{x}\right)^T \\ &= \sum_{j=1}^{N(\mathbf{x})} \left[\mathbf{P}\left(\boldsymbol{\xi}^{g(j)}, \mathbf{x}\right)^T W\left(\boldsymbol{\xi}^{g(j)}, \mathbf{x}\right) \mathbf{P}\left(\boldsymbol{\xi}^{g(j)}, \mathbf{x}\right) \right] \mathbf{Q}(\mathbf{x}), \end{aligned} \tag{2.5}$$

where $\boldsymbol{\xi}^{g(j)}$ denotes coordinates of particle $g(j)$. We notice that the difference between Eq. (2.5) and the corresponding equation in [11] is that Eq. (2.5) is obtained by summing values of functions at the particles whereas that in Ref. [11] is derived by integrating each side over the compact support of the function $W(\boldsymbol{\xi}, \mathbf{x})$. That is, unlike the approach followed

in Ref. [11], in Eq. (2.5) the mass and the mass density associated with each particle are not needed. With the definitions

$$\begin{aligned}
&\mathbf{H}(\boldsymbol{\xi},\mathbf{x}) \\
&= \left[\mathbf{P}^T\left(\boldsymbol{\xi}^{g(1)},\mathbf{x}\right),\mathbf{P}^T\left(\boldsymbol{\xi}^{g(2)},\mathbf{x}\right),\cdots,\mathbf{P}^T\left(\boldsymbol{\xi}^{g(N(\mathbf{x}))},\mathbf{x}\right)\right], \\
&\mathbf{W}(\boldsymbol{\xi},\mathbf{x}) \\
&= \begin{bmatrix} W\left(\boldsymbol{\xi}^{g(1)},\mathbf{x}\right) & 0 & \cdots & 0 \\ 0 & W\left(\boldsymbol{\xi}^{g(2)},\mathbf{x}\right) & \cdots & 0 \\ \vdots & \vdots & \ddots & 0 \\ 0 & 0 & 0 & W\left(\boldsymbol{\xi}^{g(N(\mathbf{x}))},\mathbf{x}\right) \end{bmatrix}, \\
&\mathbf{F}^{(\mathbf{x})T}(\boldsymbol{\xi},\mathbf{x}) \\
&= \left[f\left(\boldsymbol{\xi}^{g(1)}\right),f\left(\boldsymbol{\xi}^{g(2)}\right),\ldots,f\left(\boldsymbol{\xi}^{g(N(\mathbf{x}))}\right)\right], \qquad (2.6)
\end{aligned}$$

Eq. (2.5) becomes

$$\begin{aligned}
&\mathbf{H}(\boldsymbol{\xi},\mathbf{x})\,\mathbf{W}(\boldsymbol{\xi},\mathbf{x})\,\mathbf{F}^{(\mathbf{x})}(\boldsymbol{\xi},\mathbf{x}) \\
&\quad = \mathbf{H}(\boldsymbol{\xi},\mathbf{x})\,\mathbf{W}(\boldsymbol{\xi},\mathbf{x})\,\mathbf{H}^T(\boldsymbol{\xi},\mathbf{x})\,\mathbf{Q}(\mathbf{x})\,. \qquad (2.7)
\end{aligned}$$

Values of elements of matrices $\mathbf{H}(\boldsymbol{\xi},\mathbf{x})$, $\mathbf{W}(\boldsymbol{\xi},\mathbf{x})$ and $\mathbf{F}^{(\mathbf{x})}(\boldsymbol{\xi},\mathbf{x})$ depend, respectively, upon values of the matrix $\mathbf{P}(\boldsymbol{\xi},\mathbf{x})$, the kernel function $W(\boldsymbol{\xi},\mathbf{x})$ and the function f at all particles located in the compact support of $W(\boldsymbol{\xi},\mathbf{x})$ associated with point $\mathbf{x}$. Equation (2.7) can be rewritten as

$$\mathbf{C}(\boldsymbol{\xi},\mathbf{x})\,\mathbf{Q}(\mathbf{x}) = \mathbf{D}(\boldsymbol{\xi},\mathbf{x})\,\mathbf{F}^{(\mathbf{x})}(\boldsymbol{\xi},\mathbf{x}), \qquad (2.8)$$

where $\mathbf{C}(\boldsymbol{\xi},\mathbf{x}) = \mathbf{H}(\boldsymbol{\xi},\mathbf{x})\,\mathbf{W}(\boldsymbol{\xi},\mathbf{x})\,\mathbf{H}^T(\boldsymbol{\xi},\mathbf{x})$, $\mathbf{D}(\boldsymbol{\xi},\mathbf{x}) = \mathbf{H}(\boldsymbol{\xi},\mathbf{x})\,\mathbf{W}(\boldsymbol{\xi},\mathbf{x})$.

It is obvious that the matrix $\mathbf{C}(\boldsymbol{\xi},\mathbf{x})$ defined above is symmetric. That is why we call this technique the SSPH method. The set of simultaneous linear algebraic equations in Eq. (2.8) can be solved for the unknown elements of the matrix $\mathbf{Q}(\mathbf{x})$. The symmetry of the matrix $\mathbf{C}(\boldsymbol{\xi},\mathbf{x})$ reduces storage requirements and the CPU time needed to solve Eq. (2.8) for $\mathbf{Q}(\mathbf{x})$. It is interesting to note that none of the matrices in Eq. (2.8) involves derivatives of the kernel function. Thus a much larger class of functions can be used as the kernel function which improves the practicality and the usefulness of the method.

In order to show that the matrix $\mathbf{C}(\boldsymbol{\xi},\mathbf{x})$ is non-singular, we write it as

$$\begin{aligned}
\mathbf{C}(\boldsymbol{\xi},\mathbf{x}) = \Big[&W(g(1))\,\mathbf{P}^T(g(1)),\,W(g(2))\,\mathbf{P}^T(g(2)),\ldots, \\
&W(g(N(\mathbf{x})))\,\mathbf{P}^T(g(N(\mathbf{x})))\Big]\begin{bmatrix}\mathbf{P}(g(1)) \\ \mathbf{P}(g(2)) \\ \vdots \\ \mathbf{P}(g(N(\mathbf{x})))\end{bmatrix} \qquad (2.9)
\end{aligned}$$

where $W(g(1)) \equiv W(\boldsymbol{\xi}^{g(1)},\mathbf{x})$ and $\mathbf{P}^T(g(1)) \equiv \mathbf{P}^T(\boldsymbol{\xi}^{g(1)},\mathbf{x})$. Thus $\mathbf{C}(\boldsymbol{\xi},\mathbf{x})$ equals the product of a $10 \times N(\mathbf{x})$ matrix and a $N(\mathbf{x}) \times 10$ matrix. By the Binet–Cauchy Theorem [25], the determinant of the matrix $\mathbf{C}(\boldsymbol{\xi},\mathbf{x})$ is given by

$$\begin{aligned}
&Det[\mathbf{C}(\boldsymbol{\xi},\mathbf{x})] \\
&= \sum_{\substack{n_1,n_2,\ldots,n_{10}=1 \\ n_1<n_2<\cdots<n_{10}}}^{N(\mathbf{x})} \left\{ Det\left[W(g(n_1))\,\mathbf{P}^T(g(n_1)),\,W(g(n_2))\right.\right. \\
&\qquad \left.\left.\times\,\mathbf{P}^T(g(n_2)),\ldots,W(g(n_{10}))\times\mathbf{P}^T(g(n_{10}))\right]\right. \\
&\qquad \left.\times Det\begin{bmatrix}\mathbf{P}(g(n_1)) \\ \mathbf{P}(g(n_2)) \\ \vdots \\ \mathbf{P}(g(n_{10}))\end{bmatrix}\right\} \\
&= \sum_{\substack{n_1,n_2,\ldots,n_{10}=1 \\ n_1<n_2<\cdots<n_{10}}}^{N(\mathbf{x})} \left\{ \prod_{k=n_1,n_2,\ldots,n_{10}} W(g(k)) \times Det\begin{bmatrix}\mathbf{P}(g(n_1)) \\ \mathbf{P}(g(n_2)) \\ \vdots \\ \mathbf{P}(g(n_{10}))\end{bmatrix}^2 \right\}. \qquad (2.10)
\end{aligned}$$

Here $n_1, n_2, \ldots, n_{10}$ are any ten particles in the ascending order from 1 to $N(\mathbf{x})$ that are in the compact support of $W(\boldsymbol{\xi},\mathbf{x})$. Because the polynomial functions in Eq. (2.3) are linearly independent and the kernel function W is positive everywhere in its compact support, the determinant of matrix $\mathbf{C}(\boldsymbol{\xi},\mathbf{x})$ is not zero. Thus the necessary condition for the matrix $\mathbf{C}(\boldsymbol{\xi},\mathbf{x})$ to be non-singular is that the number of particles in the compact support of the kernel function equals at least the number of linearly independent monomials in Eq. (2.3). Whether the matrix $\mathbf{C}(\boldsymbol{\xi},\mathbf{x})$ is singular or not also depends on the distribution of particles in its compact support. In general, it must be ensured that at least three particles in the compact support of the kernel function do not have the same x_1, x_2 and x_3 coordinates. The proof of the statement that the matrix $\mathbf{C}(\boldsymbol{\xi},\mathbf{x})$ is non-singular is given below for the 1D case.

For a 1D problem,

$$\mathbf{P}(\boldsymbol{\xi}-\mathbf{x}) = \left[1,(\xi_1-x_1),(\xi_1-x_1)^2\right],$$

and using Vandermonde's rule [26], Eq. (2.10) reduces to

$$Det[\mathbf{C}(\boldsymbol{\xi},\mathbf{x})] = \sum_{\substack{n_1,n_2,n_3=1\\ n_1<n_2<n_3}}^{N(\mathbf{x})} \left\{ \prod_{k=n_1,n,n_3} W(g(k)) \left[\left(\xi_1^{g(n_2)} - \xi_1^{g(n_1)}\right) \times \left(\xi_1^{g(n_2)} - \xi_1^{g(n_3)}\right)\left(\xi_1^{g(n_1)} - \xi_1^{g(n_3)}\right)\right]^2 \right\}.$$

For $\xi_1^{g(n_1)} \neq \xi_1^{g(n_2)} \neq \xi_1^{g(n_3)}$, the determinant will not equal zero. Thus for the matrix $\mathbf{C}(\boldsymbol{\xi},\mathbf{x})$ to be nonsingular, the necessary and sufficient condition is that the compact support of the kernel function include at least three different particles.

For non-singular matrix $\mathbf{C}(\boldsymbol{\xi},\mathbf{x})$, the solution of Eq. (2.8) is

$$\begin{aligned}\mathbf{Q}(\mathbf{x}) &= \mathbf{C}(\boldsymbol{\xi},\mathbf{x})^{-1}\,\mathbf{D}(\boldsymbol{\xi},\mathbf{x})\,\mathbf{F}^{(\mathbf{x})}(\boldsymbol{\xi},\mathbf{x})\\ &= \mathbf{K}^{(\mathbf{x})}(\boldsymbol{\xi},\mathbf{x})\,\mathbf{F}^{(\mathbf{x})}(\boldsymbol{\xi},\mathbf{x}),\end{aligned} \tag{2.11}$$

where $\mathbf{K}^{(\mathbf{x})}(\boldsymbol{\xi},\mathbf{x}) = \mathbf{C}(\boldsymbol{\xi},\mathbf{x})^{-1}\mathbf{D}(\boldsymbol{\xi},\mathbf{x})$. We note that Eq. (2.11) is the same as Eq. (7.2) in [15] which is derived from the fast version of the generalized MLS method. Thus values of the function and of its derivatives at the point $\mathbf{x}$ are expressed in terms of values of the function at particles that lie in the compact support of the kernel function $W(\boldsymbol{\xi},\mathbf{x})$ associated with the point $\mathbf{x}$.

For the matrix $\mathbf{S}$ defined by

$$\mathbf{S} = \begin{array}{c} \\ 1 \\ 2 \\ \vdots \\ N(\mathbf{x}) \end{array} \begin{array}{c} \begin{array}{ccccccccc} 1 & \cdots & g(1) & \cdots & g(2) & \cdots & g(N(\mathbf{x})) & \cdots & M \end{array} \\ \begin{bmatrix} 0 & \cdots & 1 & \cdots & 0 & \cdots & 0 & \cdots & 0 \\ 0 & \cdots & 0 & \cdots & 1 & \cdots & 0 & \cdots & 0 \\ \vdots & \ddots & \vdots & \ddots & \vdots & \ddots & \vdots & \ddots & \vdots \\ 0 & \cdots & 0 & \cdots & 0 & \cdots & 1 & \cdots & 0 \end{bmatrix} \end{array}, \tag{2.12}$$

we note that $\mathbf{I}_{N(\mathbf{x})} = \mathbf{S}\mathbf{S}^T$, where $\mathbf{I}_{N(\mathbf{x})}$ is the $N(\mathbf{x}) \times N(\mathbf{x})$ identity matrix. Quantities on the top and on the left of the matrix are the column number and the row number, respectively, and M equals the total number of particles in the entire domain of interest. Writing Eq. (2.11) as

$$\begin{aligned}\mathbf{Q}(\mathbf{x}) &= \mathbf{K}^{(\mathbf{x})}(\boldsymbol{\xi},\mathbf{x})\,\mathbf{F}^{(\mathbf{x})}(\boldsymbol{\xi},\mathbf{x}) = \mathbf{K}^{(\mathbf{x})}(\boldsymbol{\xi},\mathbf{x})\,\mathbf{I}_{N(\mathbf{x})}\mathbf{F}^{(\mathbf{x})}(\boldsymbol{\xi},\mathbf{x}),\\ &= \left(\mathbf{K}^{(\mathbf{x})}(\boldsymbol{\xi},\mathbf{x})\mathbf{S}\right)\left(\mathbf{S}^T\mathbf{F}^{(\mathbf{x})}(\boldsymbol{\xi},\mathbf{x})\right),\end{aligned} \tag{2.13}$$

we have

$$\mathbf{K}^{(\mathbf{x})}(\boldsymbol{\xi},\mathbf{x})\mathbf{S} = \begin{array}{c} \\ 1 \\ 2 \\ \vdots \\ 10 \end{array} \begin{array}{c} \begin{array}{ccccccccc} 1 & \cdots & g(1) & \cdots & g(2) & \cdots & g(N(\mathbf{x})) & \cdots & M \end{array} \\ \begin{bmatrix} 0 & \cdots & K^{(\mathbf{x})}_{1g(1)} & \cdots & K^{(\mathbf{x})}_{1g(2)} & \cdots & K^{(\mathbf{x})}_{1g(N(\mathbf{x}))} & \cdots & 0 \\ 0 & \cdots & K^{(\mathbf{x})}_{2g(1)} & \cdots & K^{(\mathbf{x})}_{2g(2)} & \cdots & K^{(\mathbf{x})}_{2g(N(\mathbf{x}))} & \cdots & 0 \\ \vdots & \ddots & \vdots & \ddots & \vdots & \ddots & \vdots & \ddots & \vdots \\ 0 & \cdots & K^{(\mathbf{x})}_{10g(1)} & \cdots & K^{(\mathbf{x})}_{10g(2)} & \cdots & K^{(\mathbf{x})}_{10g(N(\mathbf{x}))} & \cdots & 0 \end{bmatrix} \end{array}$$

$$\mathbf{S}^T\mathbf{F}^{(\mathbf{x})}(\boldsymbol{\xi},\mathbf{x}) = \begin{array}{c} \begin{array}{ccccccccc} 1 & \cdots & g(1) & \cdots & g(2) & \cdots & g(N(\mathbf{x})) & \cdots & M \end{array} \\ \left[0 \cdots f\left(\boldsymbol{\xi}^{g(1)}\right) \cdots f\left(\boldsymbol{\xi}^{g(2)}\right) \cdots f\left(\boldsymbol{\xi}^{g(N(\mathbf{x}))}\right) \cdots 0\right]^T \end{array}$$

Because of columns of zeros in the matrix product $\mathbf{K}^{(\mathbf{x})}(\boldsymbol{\xi},\mathbf{x})\mathbf{S}$, we modify the zero elements in the matrix $\mathbf{S}^T\mathbf{F}^{(\mathbf{x})}(\boldsymbol{\xi},\mathbf{x})$ as follows while not changing the right hand side of Eq. (2.13):

$$\mathbf{S}^T\mathbf{F}^{(\mathbf{x})}(\boldsymbol{\xi},\mathbf{x}) = \begin{array}{c} \begin{array}{ccccccccc} 1 & \cdots & g(1) & \cdots & g(2) & \cdots & g(N(\mathbf{x})) & \cdots & M \end{array} \\ \left[f(\xi^1) \cdots f\left(\boldsymbol{\xi}^{g(1)}\right) \cdots f\left(\boldsymbol{\xi}^{g(2)}\right) \cdots f\left(\boldsymbol{\xi}^{g(N(\mathbf{x}))}\right) \cdots f\left(\xi^M\right)\right]^T \end{array}$$

Thus, Eq. (2.13) can be written as

$$\mathbf{Q}(\mathbf{x}) = \mathbf{K}(\boldsymbol{\xi},\mathbf{x})\,\mathbf{F}(\boldsymbol{\xi}) \tag{2.14}$$

where

$$\mathbf{K}(\boldsymbol{\xi},\mathbf{x}) = \mathbf{K}^{(\mathbf{x})}(\boldsymbol{\xi},\mathbf{x})\mathbf{S},$$
$$\mathbf{F}(\boldsymbol{\xi}) = \left[f\left(\boldsymbol{\xi}^1\right), f\left(\boldsymbol{\xi}^2\right), \ldots, f\left(\boldsymbol{\xi}^M\right)\right]^T.$$

Alternatively, we write Eq. (2.14) as

$$Q_I(\mathbf{x}) = \sum_{J=1}^{M} K_{IJ}F_J, \quad I = 1, 2, \ldots, 10,$$

where $F_J = f(\boldsymbol{\xi}^J)$. The value of the function and its derivatives at the point $\mathbf{x}$ are now expressed in terms of values of the function at all particles in the entire domain.

Three components of Eq. (2.14) when written explicitly are

$$\begin{aligned} f(\mathbf{x}) &= Q_1(\mathbf{x}) = \sum_{J=1}^{M} K_{1J}F_J,\\ \frac{\partial f(\mathbf{x})}{\partial x_1} &= Q_2(\mathbf{x}) = \sum_{J=1}^{M} K_{2J}F_J,\\ \frac{\partial^2 f(\mathbf{x})}{\partial x_1^2} &= 2Q_5(\mathbf{x}) = \sum_{J=1}^{M} 2K_{5J}F_J. \end{aligned} \tag{2.15}$$

In the terminology of the FEM functions $K_{1J}, J = 1, 2, \ldots, M$ can be viewed as shape functions for the point $\mathbf{x}$. Similarly, functions $K_{2J}, J = 1, 2, \ldots, M$ and $2K_{5J}$, $J = 1, 2, \ldots, M$ can be regarded as shape functions for

$\partial f(\mathbf{x})/\partial x_1$ and $\partial^2 f(\mathbf{x})/\partial x_1^2$, respectively. Thus shape functions for $f(\mathbf{x})$, its first derivative and its second derivative at the position $\mathbf{x}$ are different. Recall that in the FEM

$$\frac{\partial^{\alpha+\beta+\gamma}}{\partial x_1^\alpha \partial x_2^\beta \partial x_3^\gamma} f(\mathbf{x}) = \sum_{J=1}^{M} \frac{\partial^{\alpha+\beta+\gamma}}{\partial x_1^\alpha \partial x_2^\beta \partial x_3^\gamma} N_J F_J \tag{2.16}$$

For $\alpha = \beta = \gamma = 0$, Eq. (2.16) giving the approximate value of the function in the FEM is exactly of the same form as that in the SSPH method. However, expressions for approximate values of the first and the second derivatives of the function at the point $\mathbf{x}$ in the SSPH method are different from those in the FEM. In order to compute approximate values of derivatives of the function in the SSPH method, we do not need to differentiate the basis functions. Instead we use another set of basis functions. Values of coefficients in Eq. (2.15) for finding approximate values of the function $f(\mathbf{x})$, its first derivative and its second derivative at the point $\mathbf{x}$ are found simultaneously.

In the MLS method, the RKPM and the FEM one can also use a different set of shape functions to approximate the trial solution and its derivatives, but it increases the number of unknowns at a node or a particle. Here the number of unknowns per particle remains the same but one does need to have more particles in the compact support of the kernel function associated with the point $\mathbf{x}$ to simultaneously find basis for the function and its spatial derivatives in order for the matrix $\mathbf{C}(\boldsymbol{\xi}, \mathbf{x})$ defined by Eq. (2.9) to be non-singular. This can be accomplished by enlarging either the radius of the compact support of the kernel function or the number of particles in the domain which generally reduces the error in approximating the trial solution.

As in the FEM, one can determine approximate values of the derivatives of the function f at the point $\mathbf{x}$ by differentiating with respect to x_i both sides of Eq. $(2.15)_1$.

For the SSPH method, the estimates of a function, and its first and second order derivatives are consistent up to orders m, $(m-1)$ and $(m-2)$, respectively, if up to m order terms are retained in the Taylor series expansion (2.1) of the function.

The SSPH basis functions (2.14) have been derived without using any connectivity among the particles. Therefore, like the MLS basis functions [27] these can be used as basis to solve an initial-boundary-value problem. We note that like the MLS basis functions the SSPH basis functions (2.14) do not exhibit the Kronecker delta property.

3 Formulation of 2D elasto-statics problems

In rectangular Cartesian coordinates, equations of equilibrium for 2D deformations of a linear elastic body occupying the domain Ω are

$$\sigma_{ij,j} + b_i = 0, \qquad \text{in } \Omega, \quad i = 1, 2, \tag{3.1}$$

where a repeated index implies summation over the range of the index, b_i is the body force per unit volume which we take to be zero, σ_{ij} is the Cauchy stress, and a comma followed by the index j denotes partial differentiation with respect to x_j. The boundary conditions may be written as

$$\begin{aligned} &u_i = \bar{u}_i \quad \text{on } \Gamma_u \\ &t_i \equiv \sigma_{ij} n_j = \bar{t}_i \quad \text{on } \Gamma_t \end{aligned} \tag{3.2}$$

$\bar{u}_i$ is the prescribed displacement on Γ_u, and $\bar{t}_i$ the prescribed surface traction on Γ_t, $\mathbf{n} = [n_1, n_2]^T$ is the unit outward normal to the boundary Γ_t. These two boundary conditions are the well-known essential and natural boundary conditions, respectively.

The constitutive relation for a linear elastic isotropic homogeneous material is

$$\boldsymbol{\sigma} = \mathbf{D}\boldsymbol{\varepsilon} \tag{3.3}$$

where $\boldsymbol{\varepsilon} = [\varepsilon_{11}, \varepsilon_{22}, 2\varepsilon_{12}]^T$ is the strain tensor, $\boldsymbol{\sigma} = [\sigma_{11}, \sigma_{22}, \sigma_{12}]^T$ is the stress tensor, $\mathbf{D}$ given by

$$\mathbf{D} = \frac{E_0}{1-\nu_0^2} \begin{bmatrix} 1 & \nu_0 & 0 \\ \nu_0 & 1 & 0 \\ 0 & 0 & \frac{1-\nu_0}{2} \end{bmatrix} \tag{3.4}$$

is the matrix of elastic constants in which

$$\begin{aligned} &E_0 = \tfrac{E}{1-\nu^2}, \quad \nu_0 = \tfrac{\nu}{1-\nu} \quad \text{for plane strain} \\ &E_0 = E, \quad \nu_0 = \nu \quad \text{for plane stress} \end{aligned} \tag{3.5}$$

Here E is Young's modulus and ν the Poisson ratio.

The strain tensor $\boldsymbol{\varepsilon}$ is defined by

$$\boldsymbol{\varepsilon} = \mathbf{L}\mathbf{u} \tag{3.6}$$

where the differential operator matrix $\mathbf{L}$ and the displacement vector $\mathbf{u}$ are given by

$$\mathbf{L} = \begin{bmatrix} \frac{\partial}{\partial x_1} & 0 \\ 0 & \frac{\partial}{\partial x_2} \\ \frac{\partial}{\partial x_2} & \frac{\partial}{\partial x_1} \end{bmatrix}, \quad \mathbf{u} = \begin{bmatrix} u_1 \\ u_2 \end{bmatrix} \tag{3.7}$$

Equations (3.1)–(3.3) and (3.6) constitute a set of two partial differential equations for the two unknown components of displacements u_1 and u_2. We discuss below three ways of finding an approximate solution of these equations by using the SSPH basis functions.

3.1 The collocation method or approximate solution using the strong form of differential equations

We assume that there are M scattered particles located in the domain Ω. In the collocation method, Eqs. (3.1), (3.3) and

(3.6) are satisfied at every one of the M particles. Thus we have

$$\left(\frac{\partial^2}{\partial x_1^2}+\frac{1-\nu_0}{2}\frac{\partial^2}{\partial x_2^2}\right)u_1^I+\frac{1+\nu_0}{2}\frac{\partial^2}{\partial x_1\partial x_2}u_2^I=0,$$
$$\frac{1+\nu_0}{2}\frac{\partial^2}{\partial x_1\partial x_2}u_1^I+\left(\frac{1-\nu_0}{2}\frac{\partial^2}{\partial x_1^2}+\frac{\partial^2}{\partial x_2^2}\right)u_2^I=0. \quad (3.8)$$

These partial differential equations are transformed to algebraic equations by using the SSPH basis functions. For the 2D problem, Eq. (2.14) giving the SSPH basis functions reduces to

$$Q_I(\mathbf{x})=\sum_{J=1}^{M}K_{IJ}F_J,\quad I=1,2,\ldots,6, \quad (3.9)$$

and second derivatives of the function $f(\mathbf{x})$ are given by

$$\frac{\partial^2 f(\mathbf{x})}{\partial x_1^2}=2Q_4(\mathbf{x})=\sum_{J=1}^{M}2K_{4J}F_J$$
$$\frac{\partial^2 f(\mathbf{x})}{\partial x_2^2}=2Q_5(\mathbf{x})=\sum_{J=1}^{M}2K_{5J}F_J \quad (3.10)$$
$$\frac{\partial^2 f(\mathbf{x})}{\partial x_1\partial x_2}=Q_6(\mathbf{x})=\sum_{J=1}^{M}K_{6J}F_J$$

Replacing the function $f(\mathbf{x})$ in Eq. (3.10) by $u_1(\mathbf{x})$ and $u_2(\mathbf{x})$, we evaluate second order derivatives of $u_1(\mathbf{x})$ and $u_2(\mathbf{x})$ in terms of values of $u_1(\mathbf{x})$ and $u_2(\mathbf{x})$ at the M particles in the domain Ω. Substituting expressions for the second order derivatives of the displacement vector in Eq. (3.8) we get the following system of algebraic equations.

$$\sum_{J=1}^{M}\Big[2K_{4J}+(1-\nu_0)K_{5J}\Big]u_1^J+\frac{1+\nu_0}{2}\sum_{J=1}^{M}K_{6J}u_2^J=0,$$
$$\frac{1+\nu_0}{2}\sum_{J=1}^{M}K_{6J}u_1^J+\sum_{J=1}^{M}\Big[(1-\nu_0)K_{4J}+2K_{5J}\Big]u_2^J=0. \quad (3.11)$$

Equations (3.11) can be written in the matrix form as

$$\sum_{J=1}^{M}\mathbf{K}'_{IJ}\mathbf{u}^J=0, \quad (3.12)$$

where

$$\mathbf{K}'_{IJ}=\begin{bmatrix}2K_{4J}+(1-\nu_0)K_{5J} & \frac{1+\nu_0}{2}K_{6J}\\ \frac{1+\nu_0}{2}K_{6J} & (1-\nu_0)K_{4J}+2K_{5J}\end{bmatrix}.$$

The matrix $\mathbf{K}'_{IJ}$ is symmetric, but the whole matrix $\mathbf{K}'$ is not symmetric.

For a particle on the boundary Γ_u where the essential boundary condition $(3.2)_1$ is prescribed, Eq. (3.12) for that particle is replaced by

$$\sum_{J=1}^{M}\mathbf{K}'_{IJ}\mathbf{u}^J=\bar{\mathbf{u}}^I \quad (3.13)$$

where

$$\mathbf{K}'_{IJ}=\begin{bmatrix}K_{1J} & 0\\ 0 & K_{1J}\end{bmatrix},\quad \bar{\mathbf{u}}^I=\begin{bmatrix}\bar{u}_1^I\\ \bar{u}_2^I\end{bmatrix}.$$

Similarly, Eq. (3.12) for particles with the assigned natural boundary condition $(3.2)_2$ is replaced by

$$\sum_{J=1}^{M}\mathbf{K}'_{IJ}\mathbf{u}^J=\bar{\mathbf{t}}^I, \quad (3.14)$$

where

$$\mathbf{K}'_{IJ}=\frac{E_0}{1-\nu_0^2}\times\begin{bmatrix}n_1K_{2J}+\frac{1-\nu_0}{2}n_2K_{3J} & \frac{1-\nu_0}{2}n_2K_{2J}+\nu_0n_1K_{3J}\\ \nu_0n_2K_{2J}+\frac{1-\nu_0}{2}n_1K_{3J} & \frac{1-\nu_0}{2}n_1K_{2J}+\nu_0n_2K_{3J}\end{bmatrix},$$
$$\bar{\mathbf{t}}^I=\begin{bmatrix}\bar{t}_1^I\\ \bar{t}_2^I\end{bmatrix}.$$

Equations (3.12)–(3.14) are a set of simultaneous linear algebraic equations that can be solved for displacements of all M particles.

3.2 Approximate solution using a weak form of governing equations

We adopt the Meshless Local Petrov–Galerkin (MLPG) formulation [14] to find an approximate solution of the boundary-value problem governed by differential Eqs. (3.1) and (3.2). It differs from the EFG method in the following two respects. The weak form is derived over a subdomain of the body, and there is no background mesh employed to numerically evaluate domain integrals appearing in the weak formulation. As before we consider M particles scattered in domain Ω and denote the 2D vector function of compact support Ω^I, contained in Ω, associated with particle I by W_i^I where the subscript $i\,(i=1,2)$ denotes its component along the x_i-coordinate axis. We take W_1^I and W_2^I to be the Gauss function defined by

$$W(\boldsymbol{\xi}-\mathbf{x})=\begin{cases}\frac{G}{(h\sqrt{\pi})^\lambda}\left(e^{-|\boldsymbol{\xi}-\mathbf{x}|^2/h^2}-e^{-\rho^2}\right) & |\boldsymbol{\xi}-\mathbf{x}|\leqslant\rho h\\ 0 & |\boldsymbol{\xi}-\mathbf{x}|>\rho h\end{cases} \quad (3.15)$$

where h is the smoothing length, ρ the scaling factor, λ the dimensionality of the space, and G the normalizing constant determined by the condition that the integral of the kernel

function over the domain equals 1.0. The Gauss kernel function is nonzero in the region $|\boldsymbol{\xi} - \mathbf{x}| \leqslant \rho h$, which is a line in 1D with length equal to $2\rho h$, a circle in 2D of radius ρh, and a sphere in 3D of radius ρh. Taking the inner product of both sides of Eqs. (3.1) and (3.2) with the test function W_i^I, integrating the resulting scalar equations over their respective domains, and combining them together we get

$$\int_{\Omega^I} \sigma_{ij,j} W_i^I \, d\Omega - \alpha \int_{\Gamma_u^I} (u_i - \bar{u}_i) \, W_i^I \, d\Gamma = 0, \tag{3.16}$$

where α is a penalty parameter, $\Gamma_u^I = \partial\Omega^I \cap \Gamma_u$, and $\partial\Omega^I$ is the boundary of Ω^I. From Fig. 2, it is clear that Γ_u^I vanishes for inner particles and also for those particles on the boundary that are well inside Γ_t.

We note that the collocation method can be considered as a special case of Eq. (3.16) with W_i^I taken as the Dirac-delta function centered at the point $\mathbf{x}$. However, the collocation method precedes the MLPG formulation of a boundary-value problem.

The application of the divergence theorem to the derivative term in Eq. (3.16) yields

$$\int_{\partial\Omega^I} \sigma_{ij} n_j W_i^I \, d\Gamma - \int_{\Omega^I} \sigma_{ij} W_{i,j}^I \, d\Omega - \alpha \int_{\Gamma_u^I} (u_i - \bar{u}_i) \times W_i^I \, d\Gamma = 0. \tag{3.17}$$

Let $\partial\Omega^I \cap \Gamma = \Gamma_u^I + \Gamma_t^I$, where $\Gamma_t^I = \partial\Omega^I \cap \Gamma_t$ and $\Gamma_u^I = \partial\Omega^I \cap \Gamma_u$. Note that the kernel function W_i^I vanishes on the part of $\partial\Omega^I$ not shared by Γ. Thus

$$\int_{\partial\Omega^I} \sigma_{ij} n_j W_i^I d\Gamma = \int_{\partial\Omega^I \cap \Gamma} \sigma_{ij} n_j W_i^I d\Gamma. \tag{3.18}$$

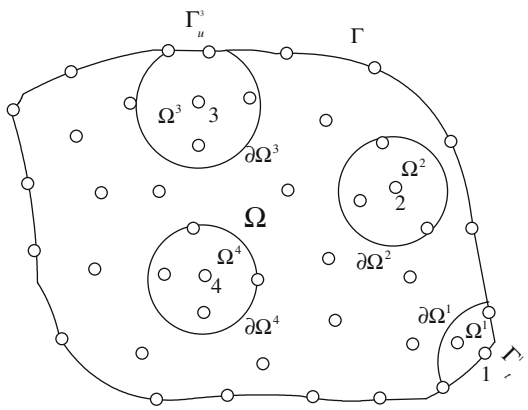

Fig. 2 Sub-domains and their boundaries for particles 1, 2, 3 and 4

Substitution from Eq. (3.18) into Eq. (3.17) gives

$$\int_{\Omega^I} \sigma_{ij} W_{i,j}^I \, d\Omega + \alpha \int_{\Gamma_u^I} u_i W_i^I \, d\Gamma - \int_{\Gamma_u^I} \sigma_{ij} n_j \, W_i^I \, d\Gamma = \int_{\Gamma_t^I} \bar{t}_i W_i^I \, d\Gamma + \alpha \int_{\Gamma_u^I} \bar{u}_i W_i^I \, d\Gamma \tag{3.19}$$

Or, in matrix form,

$$\int_{\Omega^I} (\mathbf{LM})^T \mathbf{DLu} \, d\Omega + \alpha \int_{\Gamma_u^I} \mathbf{Mu} \, d\Gamma - \int_{\Gamma_u^I} \mathbf{MNDLu} \, d\Gamma = \int_{\Gamma_t^I} \mathbf{M}\bar{\mathbf{t}} \, d\Gamma + \alpha \int_{\Gamma_u^I} \mathbf{M}\bar{\mathbf{u}} \, d\Gamma \tag{3.20}$$

where

$$\mathbf{N} = \begin{bmatrix} n_1 & 0 & n_2 \\ 0 & n_2 & n_1 \end{bmatrix} \quad \text{and} \quad \mathbf{M} = \begin{bmatrix} W^I & 0 \\ 0 & W^I \end{bmatrix}.$$

Equation (3.20) is the weak form of differential Eqs. (3.1) and boundary conditions (3.2). The order of derivatives of displacements is reduced from two to one in the weak form by introducing the first order derivatives of the test function.

As mentioned above, values of **Lu** in terms of those of **u** at the M particles in the domain Ω can be found either by differentiating the SSPH basis functions or by directly evaluating them as a part of the SSPH basis functions in which case basis functions for **Lu** and **u** are different. We use these two techniques to find an approximate solution from Eq. (3.20).

3.2.1 Approximate solution without differentiating the SSPH basis functions

Replacing the function $f(\mathbf{x})$ in Eq. (2.15) by $u_1(\mathbf{x})$ and $u_2(\mathbf{x})$ we get

$$\mathbf{u} = \sum_{J=1}^{M} \left\{ \begin{bmatrix} K_{1J} & 0 \\ 0 & K_{1J} \end{bmatrix} \mathbf{u}^J \right\}, \qquad \mathbf{Lu} = \sum_{J=1}^{M} \left\{ \begin{bmatrix} K_{2J} & 0 \\ 0 & K_{3J} \\ K_{3J} & K_{2J} \end{bmatrix} \mathbf{u}^J \right\}. \tag{3.21}$$

Substitution for **Lu** in Eq. (3.20) gives

$$\sum_{J=1}^{M} \mathbf{K'}_{IJ} \mathbf{u}^J = \mathbf{f}_I, \tag{3.22}$$

where

$$\mathbf{K}'_{IJ} = \int_{\Omega^I} (\mathbf{LM})^T \mathbf{DT}\, d\Omega + \alpha \int_{\Gamma_u^I} \mathbf{MR}\, d\Gamma - \int_{\Gamma_u^I} \mathbf{MNDT}\, d\Gamma, \tag{3.23}$$

$$\mathbf{f}_I = \int_{\Gamma_t^I} \mathbf{M}\bar{\mathbf{t}}\, d\Gamma + \alpha \int_{\Gamma_u^I} \mathbf{M}\bar{\mathbf{u}}\, d\Gamma, \tag{3.24}$$

$$\mathbf{R} = \begin{bmatrix} K_{1J} & 0 \\ 0 & K_{1J} \end{bmatrix}, \quad \mathbf{T} = \begin{bmatrix} K_{2J} & 0 \\ 0 & K_{3J} \\ K_{3J} & K_{2J} \end{bmatrix}.$$

The set of simultaneous linear algebraic Eqs. (3.22) can be solved for displacements of all particles. Subsequently, strains at any point can be computed by using Eqs. (2.15) and (3.6).

3.2.2 *Approximate solution using derivatives of SSPH basis functions*

In the FEM, the MLPG method and the RKPM, derivatives of the trial solution are usually obtained by differentiating the shape functions. Differentiating both sides of Eq. (2.14) with respect to $\mathbf{x}$ gives

$$\frac{\partial}{\partial x_\alpha}\mathbf{Q}(\mathbf{x}) = \frac{\partial}{\partial x_\alpha}\mathbf{K}(\boldsymbol{\xi}, \mathbf{x})\,\mathbf{F}(\boldsymbol{\xi}). \tag{3.25}$$

Replacing the function $f(\mathbf{x})$ in Eq. (3.25) with $\mathbf{u}(\mathbf{x})$ yields

$$\mathbf{Lu} = \sum_{J=1}^{M} \left\{ \begin{bmatrix} (\partial \mathbf{K}/\partial x_1)_{1J} & 0 \\ 0 & (\partial \mathbf{K}/\partial x_2)_{1J} \\ (\partial \mathbf{K}/\partial x_2)_{1J} & (\partial \mathbf{K}/\partial x_1)_{1J} \end{bmatrix} \mathbf{u}^J \right\}. \tag{3.26}$$

Thus Eq. (3.20) can be written as Eq. (3.22) except that now the matrix $\mathbf{T}$ is given by

$$\mathbf{T} = \begin{bmatrix} (\partial \mathbf{K}/\partial x_1)_{1J} & 0 \\ 0 & (\partial \mathbf{K}/\partial x_2)_{1J} \\ (\partial \mathbf{K}/\partial x_2)_{1J} & (\partial \mathbf{K}/\partial x_1)_{1J} \end{bmatrix}.$$

In this method, after the matrix $\mathbf{K}$ has been found, additional computations are needed to solve for derivatives of the matrix $\mathbf{K}$ with respect to x_1 and x_2.

It should be pointed out that the test function W_i^I used in Eq. (3.16) may be different from the kernel function used in Eq. (2.14) to construct the SSPH basis functions. Here, we use the same Gauss function defined in Eq. (3.15), but with different scaling factor ρ; we take $\rho = 1.0$ for the kernel function in Eq. (3.16), but use a larger value for it in Eq. (2.14) in order for the matrix $\mathbf{C}(\boldsymbol{\xi}, \mathbf{x})$ to be non-singular. In the example problems given below, we study the effect of the value of ρ in the kernel function used to construct the SSPH basis functions.

Evaluation of Integrals in Eqs. (3.23) *and* (3.24)

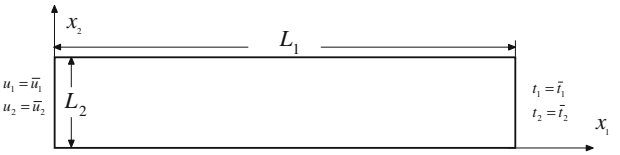

Fig. 3 A plate subjected to prescribed displacements at the left edge and surface tractions at the right edge; the top and the bottom surfaces are traction free

For the 2D problems studied herein we take the function $W(\boldsymbol{\xi}, \mathbf{x})$ to be the Gauss function defined in Eq. (3.15), set smoothing length h for particle I equal toΔ which is the smallest distance of particle I from its neighboring particles. Recalling that the Gauss function is also taken as the test function, the sub-domain Ω^I is a circle of radius ρh for particle I well inside the domain and a sector of a circle for particle I either close to or on the boundary of the domain Ω. The Gauss quadrature rule, with n_G integration points in the radial direction and $4n_G$ quadrature points in the angular direction, is employed to evaluate domain integrals in Eqs. (3.23) and (3.24). Integrals along the boundary are evaluated with n_G Gauss points.

4 Example problems

4.1 Plane stress deformations of a plate

We use the preceding formulation of an elasto-statics problem to study plane stress deformations of a plate of length $L_1 = 1.0\,\text{m}$ and width $L_2 = 0.2\,\text{m}$, with essential boundary conditions applied at the left edge and surface tractions at the remaining three edges; cf. Fig. 3. That is

$$\begin{aligned} &u_1 = \bar{u}_1, \quad u_2 = \bar{u}_2 \quad \text{on the left surface,} \\ &t_1 = 0, \quad t_2 = 0 \quad \text{on the bottom and the top surfaces,} \\ &t_1 = \bar{t}_1, \quad t_2 = \bar{t}_2 \quad \text{on the right surface.} \end{aligned} \tag{4.1}$$

The prescribed displacements at the left edge, and surface tractions at the right edge are calculated from the following analytical solution [28] that satisfies equations of equilibrium with zero body force.

$$\begin{bmatrix} u_1 \\ u_2 \end{bmatrix} = \begin{bmatrix} -\frac{2F_0}{E_0}\left(\frac{x_2}{L_2} - 0.5\right)\left[3\frac{x_1}{L_2}\left(2\frac{L_1}{L_2} - \frac{x_1}{L_2}\right) \right. \\ \left. \quad + (2+\nu_0)\frac{x_2}{L_2}\left(\frac{x_2}{L_2} - 1\right)\right] \\ \frac{2F_0}{E_0}\left[\left(\frac{x_1}{L_2}\right)^2\left(3\frac{L_1}{L_2} - \frac{x_1}{L_2}\right) \right. \\ \left. \quad + 3\nu_0\left(\frac{L_1}{L_2} - \frac{x_1}{L_2}\right)\left(\frac{x_2}{L_2} - 0.5\right)^2 + \frac{4+5\nu_0}{4}\frac{x_1}{L_2}\right] \end{bmatrix} \tag{4.2}$$

$$\begin{bmatrix}\sigma_{11}\\ \sigma_{22}\\ \sigma_{12}\end{bmatrix} = \begin{bmatrix} -12\frac{F_0}{L_2}\left(\frac{L_1}{L_2}-\frac{x_1}{L_2}\right)\left(\frac{x_2}{L_2}-0.5\right)\\ 0\\ -6\frac{F_0}{L_2}\frac{x_2}{L_2}\left(\frac{x_2}{L_2}-1\right)\end{bmatrix} \tag{4.3}$$

analytical solution but those obtained by using the collocation method differ noticeably from the analytical solution. In an attempt to give a quantitative measure of the error in the numerical solutions, we define the following relative error norm, E, in the displacements.

$$E = \left[\frac{\left|\sqrt{\int_\Omega (\mathbf{u}^{\text{compute}})^T\cdot\mathbf{u}^{\text{compute}}d\Omega}-\sqrt{\int_\Omega (\mathbf{u}^{\text{analytical}})^T\cdot\mathbf{u}^{\text{analytical}}d\Omega}\right|}{\sqrt{\int_\Omega (\mathbf{u}^{\text{analytical}})^T\cdot\mathbf{u}^{\text{analytical}}d\Omega}}\right] \tag{4.4}$$

Surface tractions $\bar{t}_1$ and $\bar{t}_2$ are determined from $\bar{t}_1=\sigma_{11}n_1+\sigma_{12}n_2$, $\bar{t}_2=\sigma_{21}n_1+\sigma_{22}n_2$. One can think of this test problem as a sophisticated patch test. Alternatively, this technique can be used to verify a code, e.g. see [29].

Values assigned to material parameters of the plate are

$$E = 226.9\,\text{GPa}, \quad \nu = 0.33$$

The parameter F_0 in Eqs. (4.2) and (4.3) is set as 10^6 N. The penalty parameter α in the weak formulation given in Eq. (3.16) is taken to be $10^5 E_0/L_1$. The problem is solved with the collocation method, i.e. Eqs. (3.12)–(3.14), and by using the weak formulation, Eq. (3.20), with the trial solution expressed in terms of the SSPH basis functions. In the latter approach, we either use Eq. $(3.21)_2$ or Eq. (3.26) for **Lu**.

Uniformly distributed 16×4 particles are placed in the plate. The scaling factor ρ for the kernel function used to generate the SSPH basis is taken as 3.0, and n_G is set equal to 10.

The deformed shape of the plate is depicted in Fig. 4 with displacements in both x_1 and x_2 directions magnified 100 times for the analytical and the numerical solutions. The labels "strong", "weak1" and "weak2" denote, respectively, results computed with the collocation method, weak formulation with **Lu** found without differentiating the SSPH basis functions, and the weak formulation with **Lu** computed by differentiating the SSPH basis functions. It is clear that, even with the coarse distribution of particles, results computed by using the weak formulation agree very well with the

In order to evaluate integrals in Eq. (4.4) over the entire domain, we use a background mesh of triangular elements and the Gauss integration rule with 13 integration points in each triangle. Since the background mesh is only used for post-processing of results, it does *not* affect the meshless nature of the computational method. The relative error norms of displacements are −0.710, −2.012 and −1.628 for the results given by the strong, weak1 and weak2 approaches. Thus the collocation method using the 2nd order partial differential equations gives the highest error, and the weak1 formulation that does not involve differentiating the SSPH basis functions has the least value of the error norm in the displacements.

We note that when the problem is solved with the collocation method, particles 1, 2, 3 and 4 located clockwise starting at the northeast corner belong to two boundaries. For example, particle 3 is on both the bottom and the left surfaces, and boundary conditions for it are

$$\begin{aligned} u_1 &= \bar{u}_1, \quad u_2 = \bar{u}_2 \quad \text{on the left surface}\\ t_1 &= 0, \quad t_2 = 0 \quad \text{on the bottom surface}\end{aligned} \tag{4.5}$$

However, only two of these four equations can be used for this particle. Results given above are for the case of the particle satisfying the two essential boundary conditions in Eq. (4.5). For the six possible choices of boundary conditions at the particle 3, the relative error norms in the displacements listed in Table 1 suggest that the relative error in the displacements is virtually the same.

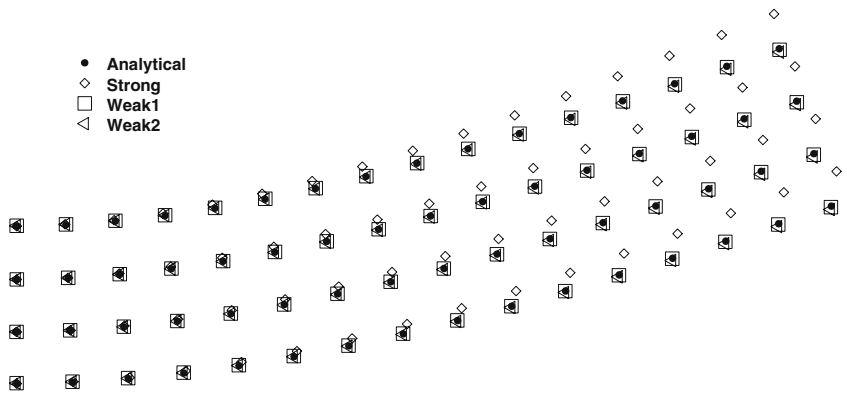

Fig. 4 Shapes of the deformed plate computed with four solution techniques (the two displacements are magnified 100 times)

Table 1 The relative error norms of displacements computed by different combinations of boundary conditions given in Eq. (4.5)

	$u_1=\bar{u}_1$ $u_2=\bar{u}_2$	$u_1=\bar{u}_1$ $t_1=0$	$u_1=\bar{u}_1$ $t_2=0$	$u_2=\bar{u}_2$ $t_2=0$	$u_2=\bar{u}_2$ $t_1=0$	$t_1=0$ $t_2=0$
$\log E$	−0.7097	−0.7092	−0.7094	−0.6955	−0.7020	−0.7049

For particles 1 and 2, there are no essential boundary conditions to be satisfied. For example, particle 1 lies on the right and the top surfaces, and pertinent boundary conditions are

$$\begin{aligned} &\sigma_{21}=0, \quad \sigma_{22}=0 \quad \text{on the top surface} \\ &\sigma_{11}=0, \quad \sigma_{12}=0 \quad \text{on the right surface} \end{aligned} \tag{4.6}$$

Because of the symmetry of the stress tensor, there are three conditions to be satisfied but we can choose only two equations out of the three listed in Eq. (4.6). Results discussed above are with $\sigma_{11}=0$ and $\sigma_{22}=0$. The relative error norm in displacements for boundary conditions $\sigma_{12}=0, \sigma_{22}=0$ is −0.6319, that for $\sigma_{11}=0, \sigma_{12}=0$ equals −0.7501, and for $\sigma_{11}=0$ and $\sigma_{22}=0$ it is −0.7097. The difference in the error norms is much larger than that when different combinations of boundary conditions at particle 3 were employed. One possible reason for boundary conditions $\sigma_{11}=0$ and $\sigma_{12}=0$ to give the smallest value of the error norm is that $\sigma_{22}=0$ for the analytical solution, and has very small values in the numerical solution. Thus all three boundary conditions in Eq. (4.6) are satisfied when we impose $\sigma_{11}=0$ and $\sigma_{12}=0$ at particle 1. It is difficult to propose a criterion for selecting the most appropriate boundary conditions for a particle at a corner. However, one can safely say that the essential boundary conditions be satisfied first. We have listed in Table 2 values of error norms for different number of particles in the plate. It is clear that boundary conditions $\sigma_{11}=0$ and $\sigma_{12}=0$ yield the smallest value of the error norm. Results presented and discussed below are with these boundary conditions at particle 1.

For the uniform 16×4 distribution of particles in the plate Figs. 5 and 6 depict, respectively, the variation of the displacement u_2 along the bottom surface, and the dimensionless stress $\sigma_{11}/(F_0/L_2)$ along the top surface of the plate for the analytical and the three numerical solutions. These also evince that the collocation method using the strong form of the problem formulation gives the largest deviation in the displacement and the axial stress from their analytical values. The maximum error in u_2 for solutions with the strong, the weak1 and the weak2 formulations equals 19.51, 1.06 and 2.34%.

Table 2 Effect of the number of particles on the relative error norms of displacements computed by different combinations of natural boundary conditions at particle 1

	$\sigma_{11}=0,\ \sigma_{12}=0$	$\sigma_{12}=0,\ \sigma_{22}=0$	$\sigma_{11}=0,\ \sigma_{22}=0$
16×4	−0.7501	−0.6319	−0.7097
31×7	−1.215	−1.146	−1.195
61×13	−1.814	−1.776	−1.804
91×19	−2.166	−2.140	−2.159

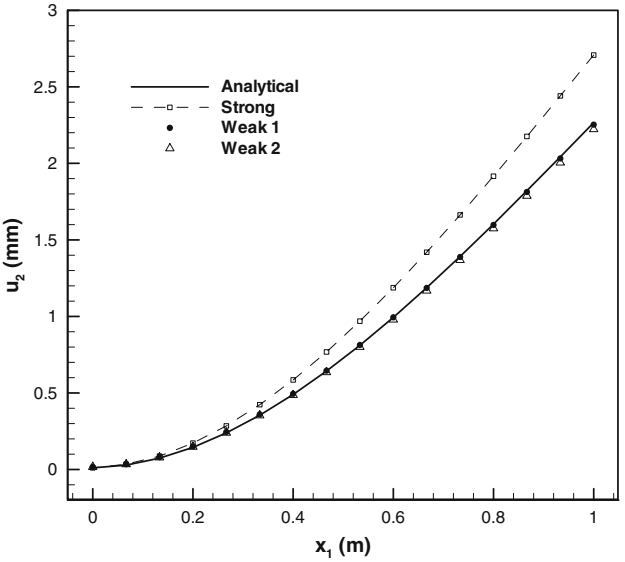

Fig. 5 Comparison of the displacement u_2 along the bottom surface of the plate computed by the strong and the two weak formulations with that obtained from the analytical solution

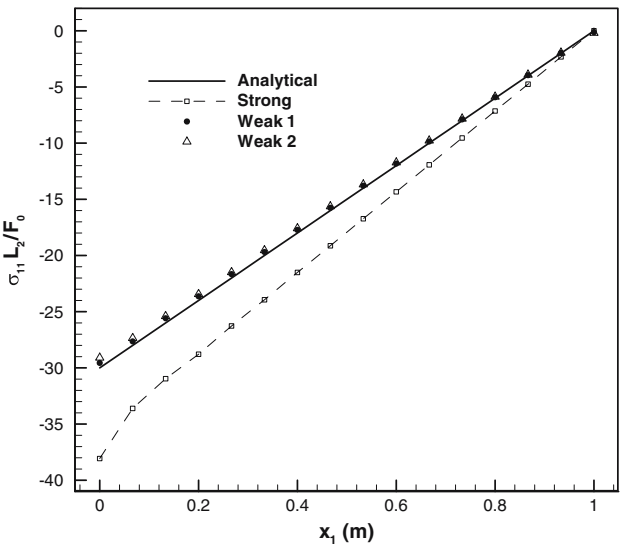

Fig. 6 Comparison of the dimensionless stress $\sigma_{11}L_2/F_0$ along the top surface of the plate computed by the strong and the two weak formulations with that obtained from the analytical solution

For Poisson's ratio = 0.499999, the variation on the bottom surface of the displacement u_2 plotted in Fig. 7 illustrates that there is no volumetric locking in any one of the three formulations.

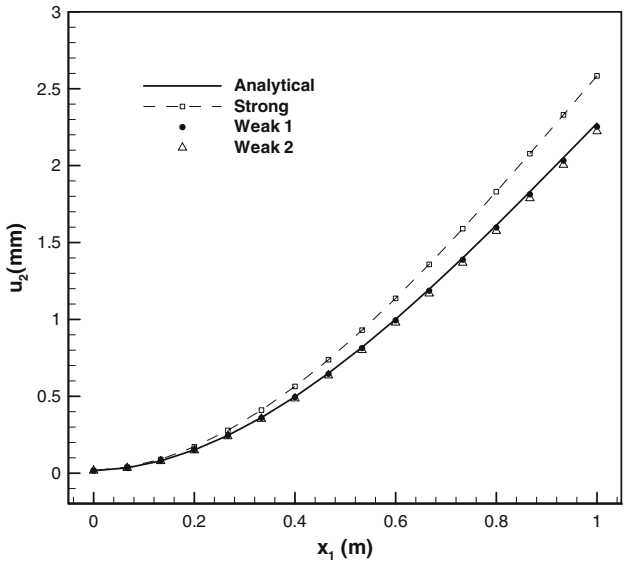

Fig. 7 Comparison of the displacement u_2 along the bottom surface of the plate computed by the strong and the two weak formulations with that obtained from the analytical solution when the Poisson ratio is increased to $\nu = 0.499999$

4.1.1 *Effect of number of Gauss points in the radial direction, n_G*

When a weak formulation is used to analyze the problem, the number of Gauss points used to numerically evaluate domain integrals in Eq. (3.23) will very likely influence the error in the computed solution of the problem. Very few integration points will not evaluate these integrals accurately, and too many Gauss points will increase the CPU time even though they will give accurate values of integrals. Figure 8 shows the change in the relative error norm of displacements with an increase in the number, n_G, of Gauss points in the radial direction. In every case $4\,n_G$ Gauss points are employed in the angular direction, and n_G Gauss points for integration on a boundary. For the two weak formulations, the relative error norm of displacements decreases with an increase in the value of n_G. However, the decrease is monotonic for the weak1 formulation and somewhat oscillatory for the weak 2 formulation. When n_G is increased from 10 to 32 the relative error norm in displacements decreases by 0.36 and 0.49% for the weak1 and the weak 2 formulations, respectively; thus ten Gauss points in the radial direction should suffice for all practical purposes.

4.1.2 *Effect of the scaling factor ρ for the kernel function used to generate the SSPH basis functions*

When generating the SSPH basis functions enough particles should be included in the kernel function's compact support in order for the matrix $\mathbf{C}(\boldsymbol{\xi}, \mathbf{x})$ to be non-singular. Thus for a 2D problem requiring the evaluation of 2nd order derivatives for the collocation method, the scaling factor ρ should be large enough to have at least six particles in the kernel function's compact support. The effect of the scaling factor ρ on the relative error norm of displacements is illustrated by plots given in Fig. 9. For each one of the three numerical solutions, the relative error norm in displacements first decreases rapidly with an increase in the value of ρ, reaches its minimum value before becoming stable for ρ greater than 3.5. A larger value of ρ is not recommended because the CPU time required to compute SSPH basis functions increases with an increase in the value of ρ. Henceforth,

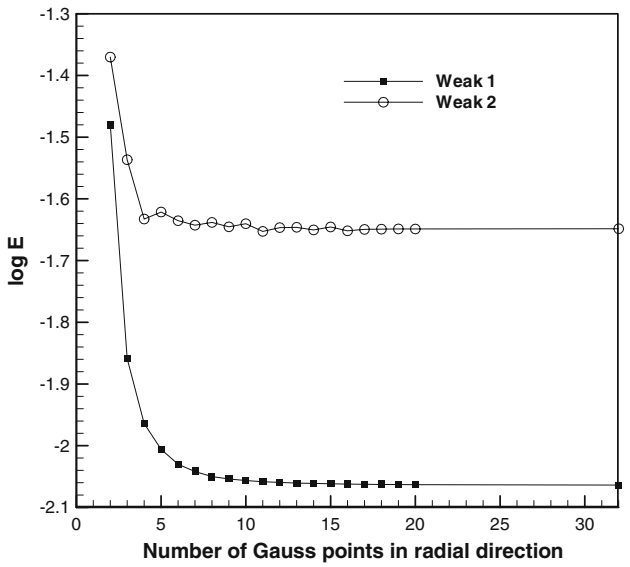

Fig. 8 Variation of the relative error norm of displacements with the number of Gauss points in the radial direction

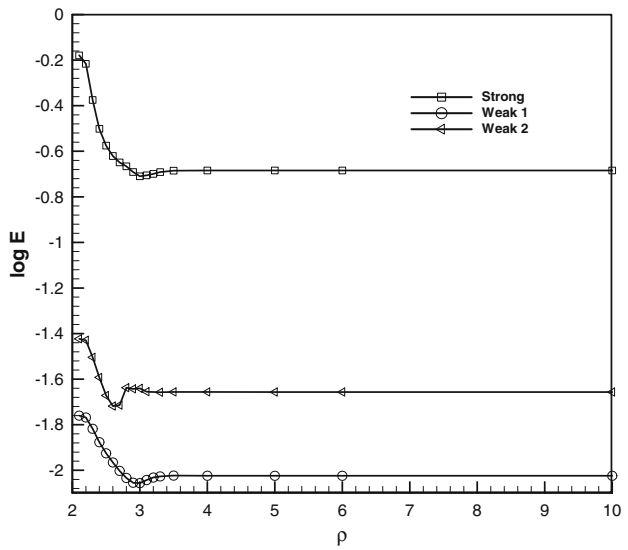

Fig. 9 Variation of the relative error norm of displacements with the scaling factor, ρ

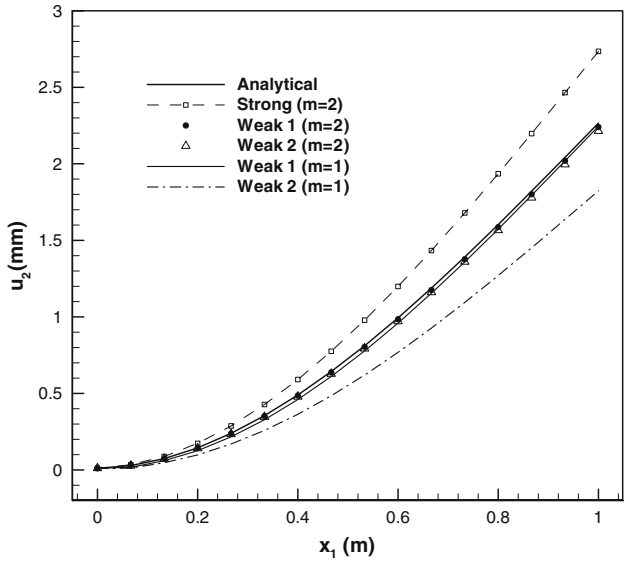

Fig. 10 Comparison of the displacement u_2 along the bottom surface for different orders ($m = 2$ and $m = 1$) of monomials used to generate SSPH basis functions

we fix the scaling factor to be 4.0 rather than 3.0 used in results presented above.

4.1.3 Effect of the number, m, of the terms retained in the Taylor series expansion

In the collocation method, Eq. (3.8) involves the second order derivatives of displacements. Thus in the SSPH basis at least up to 2nd order terms must be retained in the Taylor series expansion, Eq. (2.1), i.e., $m = 2$. For a 2D problem, the matrix $\mathbf{C}(\boldsymbol{\xi}, \mathbf{x})$ defined in Eq. (2.8) is 6×6. However, the weak formulations involve only first order derivatives of displacements and we may retain only three terms ($m = 1$) in the Taylor series resulting in a 3×3 $\mathbf{C}(\boldsymbol{\xi}, \mathbf{x})$ matrix. Figure 10 gives the variation of the displacement u_2 along the bottom surface computed by the two weak formulations with $m = 1$ and $m = 2$, the collocation method, and the analytical solution. It can be seen that the results from the weak2 formulation with $m = 1$ and from the collocation method are worse than those computed with the weak1 formulation with $m = 1$ or 2. In fact the weak1 formulation that does not necessitate differentiating the SSPH basis functions gives very good values of displacements even when $m = 1$. For the weak1 formulation the relative error norm of displacements changes from -1.743 to -1.980 when m is increased from 1 to 2, and for the weak2 formulation the corresponding values of the error norms are -0.683 and -1.638. However, when comparing results computed from the three formulations, we use the same number, 6, of terms in the Taylor series expansion, Eq. (2.1).

4.1.4 Effect of the number of particles

In Fig. 11, we have exhibited the variation of the displacement u_2 on the bottom surface of the plate for uniform particle placements of 16×4, 31×7, 61×13 and 91×19. For each

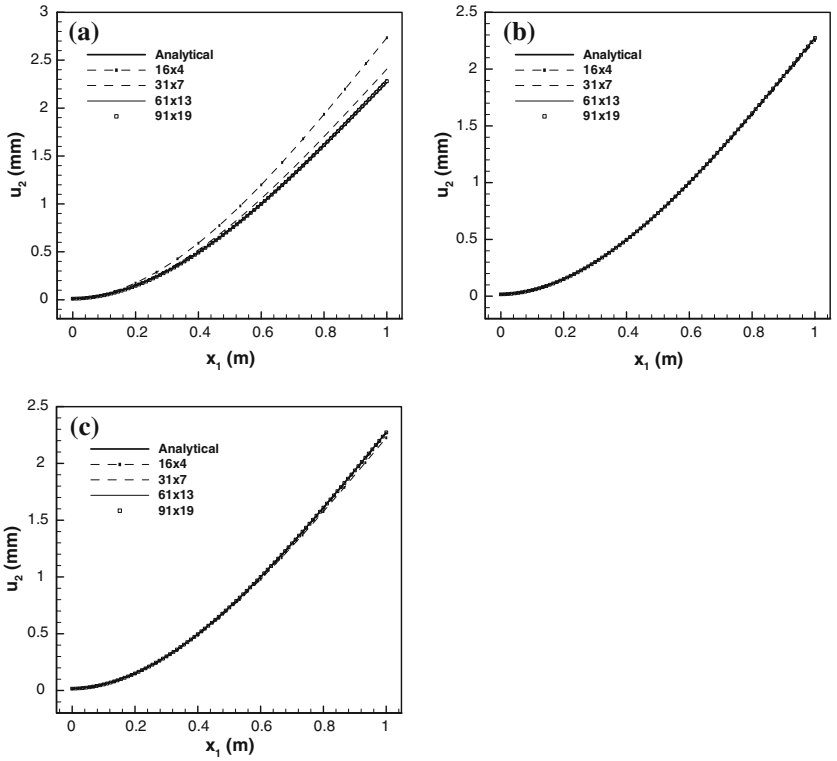

Fig. 11 Effect of particle number on the displacement u_2 along the bottom surface of the plate computed with the **a** strong formulation, **b** weak1 formulation without differentiating the SSPH basis functions, and **c** weak2 formulation with differentiating the basis functions

one of the three numerical solutions, the maximum difference in the computed and the analytical values of u_2 decreases with an increase in the number of particles. For the 61×13 uniform locations of particles, the displacement computed from the collocation method is virtually indistinguishable from that for the analytical solution. However, the two weak formulations give accurate values of the displacement even for 16×4 particles.

Figure 12 reveals the variation of the relative error norm with the logarithm of the distance between two adjacent particles. The weak1 formulation that does not require differentiating the SSPH basis functions always gives the smallest relative error norm of displacements while the collocation method using the strong form of equations gives the largest. The higher accuracy of the weak1 formulation is obtained at the cost of additional CPU time consumed in evaluating numerically the domain integrals. It can be seen that the convergence rates for the three methods are nearly the same.

4.2 Stress concentration in a plate

We use the three methods to analyze deformations in a homogeneous and isotropic linear elastic semi-infinite plate with a circular hole at its center and loaded as shown in Fig. 13. As for the previous problem surface tractions computed from the analytical solution

$$\begin{aligned}
\sigma_{rr} &= \frac{\sigma_0}{2}\left(1-\frac{b^2}{r^2}\right)+\frac{\sigma_0}{2}\left(1+3\frac{b^4}{r^4}-4\frac{b^2}{r^2}\right)\cos 2\theta \\
\sigma_{\theta\theta} &= \frac{\sigma_0}{2}\left(1+\frac{b^2}{r^2}\right)-\frac{\sigma_0}{2}\left(1+3\frac{b^4}{r^4}\right)\cos 2\theta \\
\sigma_{r\theta} &= -\frac{\sigma_0}{2}\left(1-3\frac{b^4}{r^4}+2\frac{b^2}{r^2}\right)\sin 2\theta
\end{aligned} \tag{4.7}$$

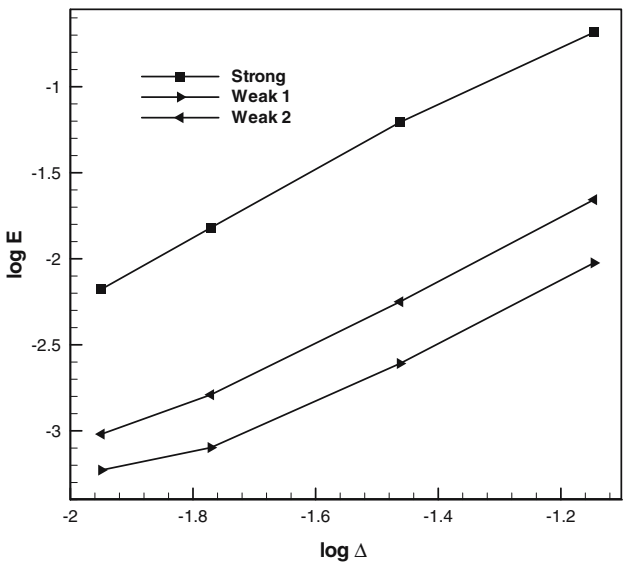

Fig. 12 Effect of the particle distance on the relative error norm of displacements computed with the strong and the two weak formulations

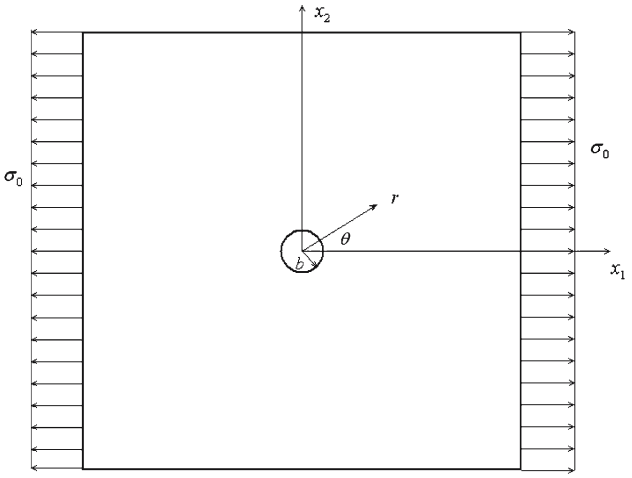

Fig. 13 Schematic sketch of a plate with a central hole and loaded in tension at two opposite edges

$$\begin{aligned}
u_1 &= \frac{1+\nu_0}{E_0}\sigma_0\left(\frac{1}{1+\nu_0}r\cos\theta+\frac{2}{1+\nu_0}\frac{b^2}{r}\cos\theta\right. \\
&\qquad \left.+\frac{1}{2}\frac{b^2}{r}\cos 3\theta-\frac{1}{2}\frac{b^4}{r^3}\cos 3\theta\right) \\
u_2 &= \frac{1+\nu_0}{E_0}\sigma_0\left(\frac{-\nu_0}{1+\nu_0}r\sin\theta-\frac{1-\nu_0}{1+\nu_0}\frac{b^2}{r}\sin\theta\right. \\
&\qquad \left.+\frac{1}{2}\frac{b^2}{r}\sin 3\theta-\frac{1}{2}\frac{b^4}{r^3}\sin 3\theta\right)
\end{aligned} \tag{4.8}$$

are applied to boundaries of the plate. In Eq. (4.7) and (4.8), (r, θ) are the cylindrical coordinates of a point with the origin at the center of the hole, and u_1 and u_2 are components, respectively, of the displacement vector $\mathbf{u}$ along the horizontal and the vertical directions. Due to the symmetry of the problem about the horizontal and the vertical centroidal axes, we analyze deformations of a quarter of the finite domain shown in Fig. 14a, and assume that a plane strain state of deformation prevails in the plate. Boundary conditions in rectangular Cartesian coordinates are listed below:

$$\begin{aligned}
&u_1 = 0, \quad t_2 = 0 \quad \text{on boundary 1} \\
&t_1 = 0, \quad t_2 = 0 \quad \text{on boundary 2} \\
&t_1 = 0, \quad u_2 = 0 \quad \text{on boundary 3} \\
&t_1 = \bar{t}_1, \quad t_2 = \bar{t}_2 \quad \text{on boundaries 4 and 5}
\end{aligned} \tag{4.9}$$

Surface tractions $\bar{t}_1$ and $\bar{t}_2$ on boundaries are determined from $\bar{t}_1 = \sigma_{11}n_1 + \sigma_{12}n_2, \bar{t}_2 = \sigma_{21}n_1 + \sigma_{22}n_2$ where $\boldsymbol{n}$ is a unit outward normal to the boundary, t is the traction vector, and values of σ_{11}, σ_{22} and σ_{12} are found from the analytical solution (4.7) by using tensor transformation rules.

Figure 14b depicts the placement of 188 particles in the domain of study with 11 particles on the quarter of the circular hole. The distribution of particles gets coarser with an increase in the distance from the circular hole. The smoothing length $h_i = \Delta_i$ where Δ_i is the smallest distance between particle i and other particles in the compact support of the

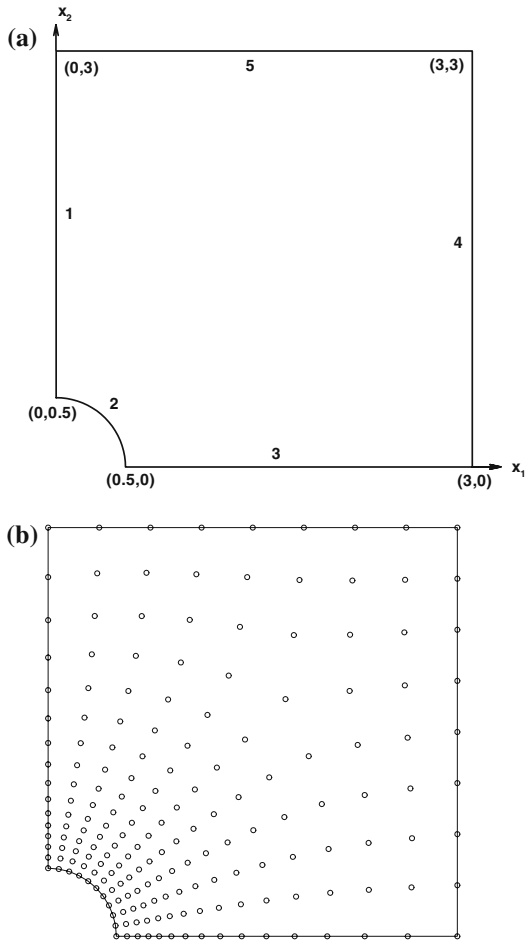

Fig. 14 **a** Schematic sketch of a quarter of the plate used in the simulation. **b** Locations of particles in the domain studied

kernel function associated with particle i. The scaling factor ρ is taken to be 4.0. The penalty parameter is set as $10^5 E_0/3$. Values assigned to material parameters of the plate and the tensile traction are

$$E = 226.9\,\text{GPa}, \quad \nu = 0.33, \quad \sigma_0 = 1\,\text{GPa}$$

Figure 15 shows contour plots of the two displacement components derived from the analytical solution and the three numerical solutions. For the collocation method, the maximum of the absolute values of deviations from the analytical solution of displacements u_1 and u_2 equal 0.183 and 0.405 mm, respectively. For the weak1 formulation the corresponding values are 0.065 and 0.047 mm, and for the weak 2 formulation they equal 0.088 and 0.075 mm, respectively. For the solution computed with the collocation method and the weak 2 formulation, the largest deviation in the value of u_1 occurs at a point near $x_2 = 0$, while the largest difference in u_2 occurs at a point close to $x_1 = 0$. However, for results computed with the weak1 formulation, places where the largest differences in the values of u_1 and u_2 occur are close to the circular hole. The relative error norms of displacements are -1.926, -3.149 and -2.293 for the three numerical methods.

Along the x_2-axis, the analytical solution gives

$$u_2|_{\theta=\pi/2} = \frac{1+\nu_0}{E_0}\sigma_0\left(\frac{-\nu_0}{1+\nu_0}x_2 - \frac{1-\nu_0}{1+\nu_0}\frac{b^2}{x_2} - \frac{1}{2}\frac{b^2}{x_2} + \frac{1}{2}\frac{b^4}{x_2^3}\right),$$
$$\left.\frac{\sigma_{11}}{\sigma_0}\right|_{\theta=\pi/2} = 1 + \frac{1}{2}\frac{b^2}{r^2} + \frac{3}{2}\frac{b^4}{r^4}. \tag{4.10}$$

Thus, the stress concentration factor equals 3.0, and is independent of values assigned to the elastic constants. Variations of the displacement u_2 for the four solutions along the x_2-axis are exhibited in Fig. 16. It is clear that at every point on the x_2-axis the displacement u_2 given by the weak1 formulation is closer to the analytic solution than that obtained from the other two methods. Figure 17 displays numerical results of the dimensionless stress σ_{11}/σ_0 along the x_2-axis. Again results from the weak1 formulation are closest to those derived from the analytical solution. The stress concentration factors determined from solutions with the collocation method and the weak1 and the weak 2 formulations equal 3.173, 3.002 and 3.148, respectively.

Figure 18 exhibits the placement of 686 particles with 21 particles on the quarter of the circle, and Fig. 19 compares the displacement u_2 computed with this placement of particles with that found from the analytical solution of the problem. The results are much closer to the analytical solution compared to those given by 188 particles. The relative error norms of displacements are -2.243, -3.260 and -2.691 for results computed with the collocation method, and the weak1 and the weak2 formulations, respectively, indicating that the solution is improved by increasing the number of particles. The corresponding values of the non-dimensional stress σ_{11}/σ_0 along the x_2-axis, exhibited in Fig. 20, reveal that the four sets of values are very close to each other. The stress concentration factors, 3.084, 2.996 and 3.037, predicted by the three numerical solutions are very close to the analytical value of 3.0. The weak1 formulation not requiring the differentiation of the SSPH basis functions still gives the best prediction of the stress concentration factor with only 0.13% difference between the numerical and the analytical values.

4.3 Comments on the comparison of solutions with the meshless method and the FEM

We have not developed our own FE code to solve either one of the two aforestated problems. There are several commercial codes that can be used to find an approximate solution of these problems. However, it will not be fair to compare the CPU time needed for a commercial code and our code using the meshless method since commercial codes have

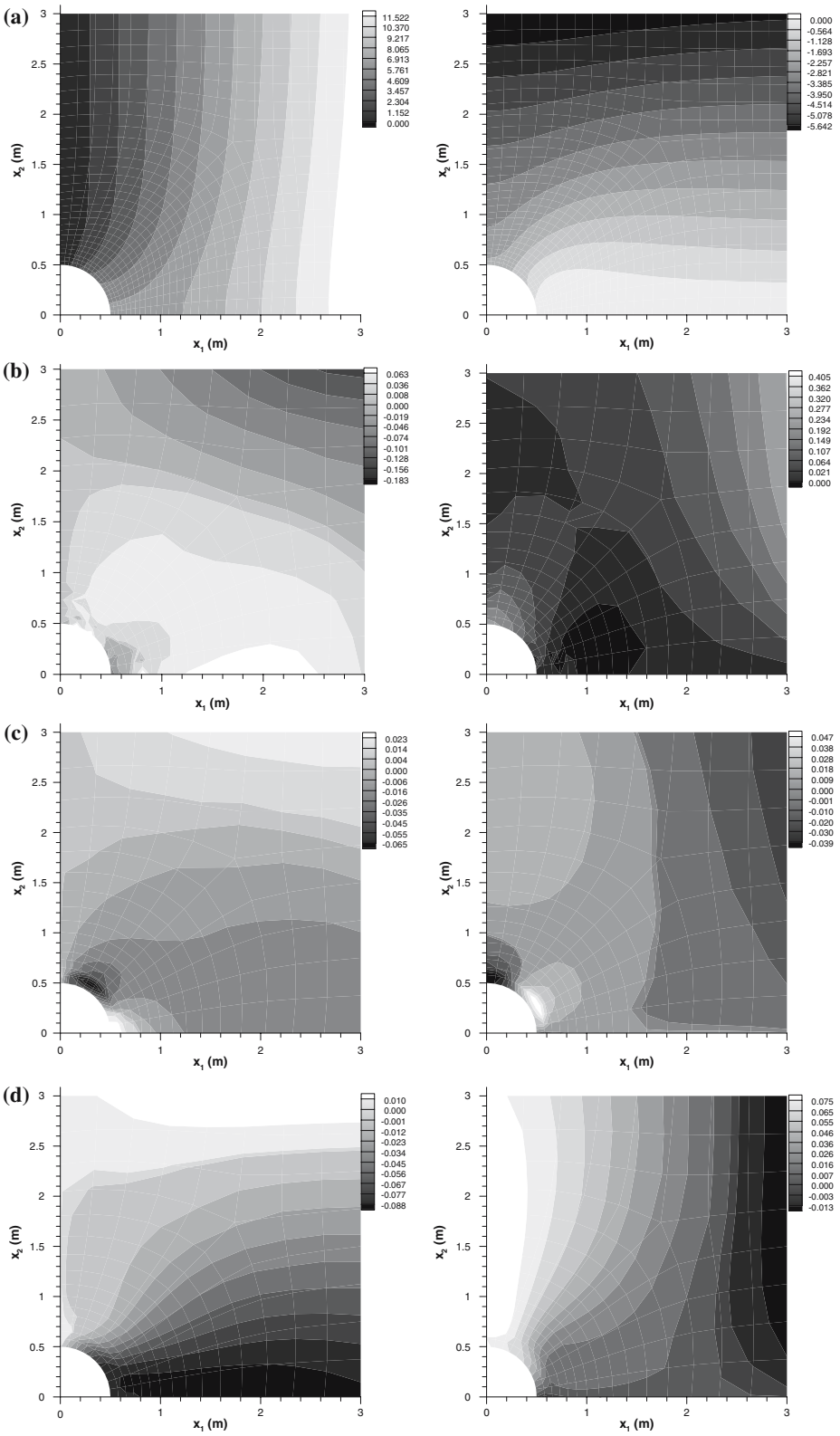

Fig. 15 Contour plots of **a** analytical values of u_1 and u_2, and of the difference between the numerical and the analytical solutions computed with **b** the strong formulation, and the weak formulations **c** without and **d** with differentiating the SSPH basis functions

been optimized while our code is basically a research tool. Our experience [22,30–35] in solving numerically boundary-value and initial-boundary-value problem suggests that at present the FEM is more efficient to analyze such problems than a meshless method. It is primarily due to a large number of Gauss points required to numerically evaluate domain

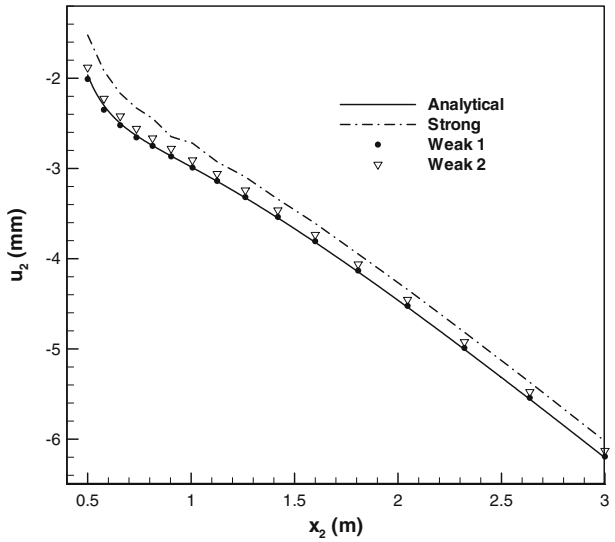

Fig. 16 Comparison of the displacement u_2 along the x_2-axis in a plate with a circular hole at its center computed by the strong and the two weak formulations with that obtained from the analytical solution

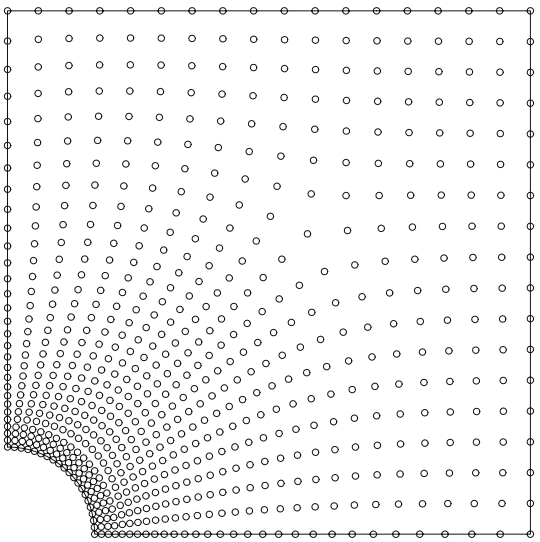

Fig. 18 Placement of 686 particles in the domain with 21 particles on the quarter of the circle

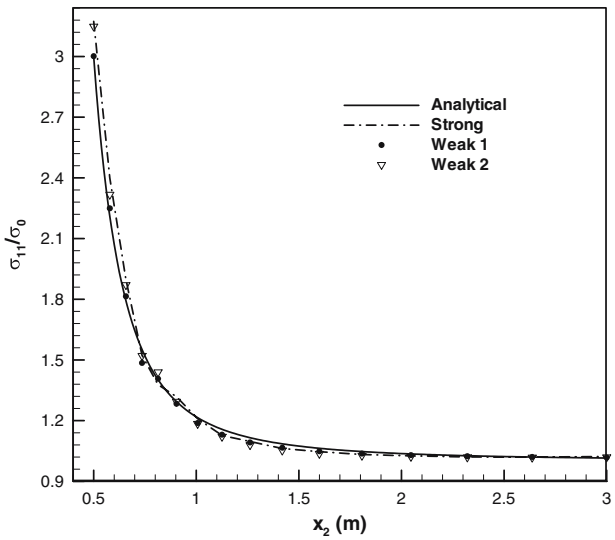

Fig. 17 Comparison of the non-dimensional stress σ_{11}/σ_0 along the x_2-axis in a plate with a circular hole computed by the strong and the weak formulations with that obtained from the analytical solution

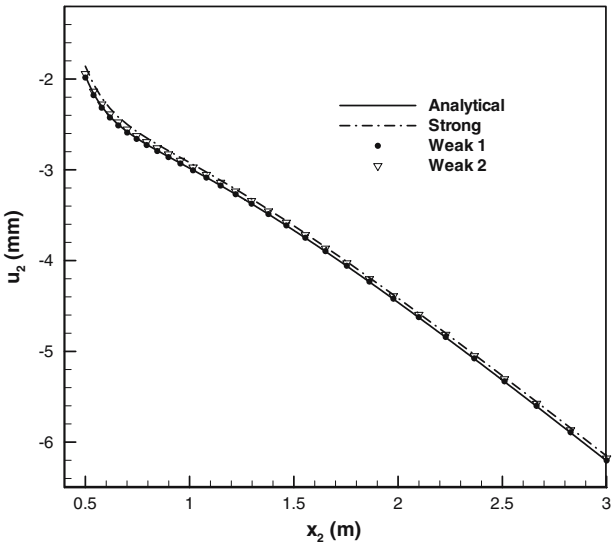

Fig. 19 Comparison of the displacement u_2 along the x_2-axis in a plate with a circular hole computed by the strong and the two weak formulations with that obtained from the analytical solution

integrals. Advantages of meshless methods include savings in personnel effort required to generate a mesh, and a better resolution of problems involving singularities. The radial basis functions (e.g. see [24]) satisfying the Kronecker delta property facilitate the satisfaction of essential boundary conditions when using a meshless method but still require more CPU time than the FEM.

5 Conclusions

We have presented a SSPH method to find basis functions using only locations of particles and termed them the SSPH basis. For approximating the function itself these basis are similar to those used in the finite element method (FEM). However, the two sets of basis differ when spatial derivatives of the function are to be approximated. Whereas in the FEM spatial derivatives of the function are derived by differentiating the basis functions, those in the SSPH method can be obtained without differentiating the SSPH basis functions. Rather one uses a kernel function different from that employed to deduce the SSPH basis functions. This is advantageous since it requires less CPU time and weak formulations using them yield more accurate solutions. In the proposed SSPH method approximate values of the function and its derivatives can be found simultaneously by solving a

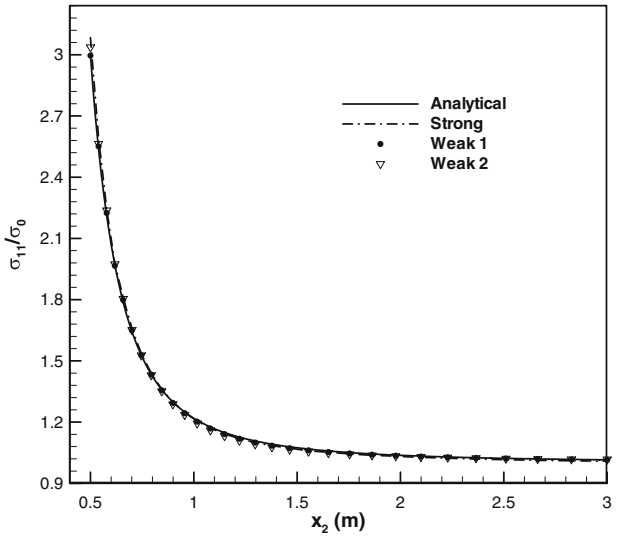

Fig. 20 Comparison of the non-dimensional stress σ_{11}/σ_0 along the x_2-axis in a plate with a circular hole computed by the strong and the two weak formulations with that obtained from the analytical solution

system of linear algebraic equations. Since only coordinates of particles are used to find the SSPH basis functions, the method is meshless like the moving least squares method, the RKPM and the MSPH.

The SSPH basis functions are employed to numerically solve two elliptic boundary-value problems by using either the collocation method or the weak formulation of the problems. Whereas the collocation method is based on the strong form of the elliptic boundary-value problem in the sense that the 2nd order partial differential equations are satisfied at discrete particles, the weak formulation involves derivatives of order one only. These 1st order derivatives are obtained either by differentiating the SSPH basis functions or without differentiating them; the former is termed weak2 and the latter weak1 formulation. Numerical experiments with two elastostatic problems have revealed that, for the same placement of particles, the error in the numerical solution computed with the weak1 formulation is least of the errors in the three solutions. The weak formulation requires more CPU time than the collocation method because of the need to numerically evaluate domain integrals appearing in the weak formulation of the problem.

Numerical experiments have also been carried out to delineate the effect of the number of particles, the least spacing between any two adjacent particles, the order of complete monomials used to generate the SSPH basis functions, the number of Gauss points employed to evaluate domain integrals, and the radius of the compact support of the kernel function used to generate the SSPH basis functions. These numerical experiments suggest that when evaluating integrals over a circular domain, one should use at least 10 and 40 Gauss points in the radial and the circumferential directions. Since in our numerical experiments the number of Gauss points in the circumferential direction always equaled four times those in the radial direction, the suggested number of Gauss points in the circumferential direction is not necessarily the optimum. A good value of the scaling factor to be used in the kernel function for the SSPH basis is 4.0. When employing the weak formulation of 2nd order elliptic boundary-value problems, one can retain only three terms in the Taylor series expansion of a function to generate the SSPH basis since results from them are as good as those when six terms are kept in the Taylor series expansion.

Based on the results of two numerical examples we recommend that the weak form without differentiating the SSPH basis functions be adopted for solving linear elastic problems.

Acknowledgments This work was partially supported by the ONR grant N00014-06-1-0567 to Virginia Polytechnic Institute and State University (VPI&SU) with Dr Y. D. S. Rajapakse as the program manager. Views expressed herein are those of authors, and neither of the funding agency nor of VPI&SU.

References

1. Lucy LB (1977) A numerical approach to the testing of the fission hypothesis. Astron J 82:1013–1024
2. Chen JK, Beraun JE, Jin CJ (1999) An improvement for tensile instability in smoothed particle hydrodynamics. Comput Mech 23:279–287
3. Chen JK, Beraun JE, Jin CJ (1999) Completeness of corrective smoothed particle method for linear elastodynamics. Comput Mech 24:273–285
4. Liu WK, Jun S, Zhang YF (1995) Reproducing kernel particle methods. Int J Num Meth Fluids 20:1081–1106
5. Liu WK, Jun S, Li S, Adee J, Belytschko T (1995) Reproducing kernel particle methods for structural dynamics. Int J Num Meth Eng 38:1655–1679
6. Chen JS, Pan C, Wu CT, Liu WK (1996) Reproducing kernel particle methods for large deformation analysis of non-linear structures. Comput Method Appl Mech Eng 139:195–227
7. Zhang GM, Batra RC (2004) Modified smoothed particle hydrodynamics method and its application to transient problems. Comput Mech 34:137–146
8. Batra RC, Zhang GM (2004) Analysis of adiabatic shear bands in elasto-thermo- viscoplastic materials by modified smoothed-particle hydrodynamics (MSPH) method. J Comput Phys 201:172–190
9. Zhang GM, Batra RC (2007) Wave propagation in functionally graded materials by modified smoothed particle hydrodynamics (MSPH) method. J Comput Phys 222:374–390
10. Batra RC, Zhang GM (2007) Search algorithm, and simulation of elastodynamic crack propagation by modified smoothed particle hydrodynamics (MSPH) method. Comput Mech 40:531–546
11. Zhang GM, Batra RC (2006) Symmetric smoothed particle hydrodynamics (SSPH) method and its application to 2-D elastic problems (submitted)
12. Belytschko T, Lu YY, Gu L, Tabbara M (1995) Element-free Galerkin methods for static and dynamic fracture. Int J Solids Struct 32:2547–2570
13. Belytschko T, Lu YY, Gu L (1994) Element-free Galerkin methods. Int J Num Meth Eng 37:229–256

14. Atluri SN, Kim H-G, Cho JY (1999) A critical assessment of the truly Meshless Local Petrov–Galerkin (MLPG), and Local Boundary Integral Equation (LBIE) methods. Comput Mech 24:348–372
15. Kim DW, Liu WK (2006) Maximum principle and convergence analysis for the meshfree point collocation method. SIAM J Numer Anal 44:515–539
16. Kim DW, Yoon YC, Liu WK, Belytschko T (2007) Extrinsic meshfree approximation using asymptotic expansion for interfacial discontinuity of derivative. J Comput Phys 221:370–394
17. Li SF, Liu WK (1999) Reproducing kernel hierarchical partition of unity, part I—formulation and theory. Int J Num Meth Eng 45:251–288
18. Li SF, Liu WK (1999) Reproducing kernel hierarchical partition of unity, part II—applications. Int J Num Meth Eng 45:289–317
19. Belytschko T, Krongauz Y, Dolbow J, Gerlach C (1998) On the completeness of meshfree particle methods. Int J Num Meth Eng 43:785–819
20. Gunther F, Liu WK, Diachin D, Christon MA (2000) Multi-scale meshfree parallel computations for viscous, compressible flows. Comput Methods Appl Mech Eng 190:279–303
21. Ferreira AJM (2003) Thick composite beam analysis using a global meshless approximation based on radial basis functions. Mech Adv Mater Struct 10:271–284
22. Qian LF, Batra RC, Chen LM (2003) Elastostatic deformations of a thick plate by using a higher-order shear and normal deformable plate theory and two meshless local Petrov–Galerkin (MLPG) methods. CMES Comput Model Eng Sci 4:161–175
23. Batra RC, Porfiri M, Spinello D (2004) Treatment of material discontinuity in two meshless local Petrov–Galerkin (MLPG) formulations of axisymmetric transient heat conduction. Int J Num Meth Eng 61:2461–2479
24. Xiao JR, McCarthy MA (2003) A local Heaviside weighted meshless method for two-dimensional solids using radial basis functions. Comput Mech 31:301–315
25. Lancaster P (1969) Theory of matrices. Academic, New York
26. David PJ (1963) Interpolation and approximation. Dover Publications, New York
27. Lancaster P, Salkauskas K (1981) Surface generated by moving least squares method. Math Comput 37:141–158
28. Timoshenko SP, Goodier JN (1970) Theory of elasticity, 3rd edn. McGraw-Hill, New York
29. Batra RC, Liang XO (1997) Finite dynamic deformations of smart structures. Comput Mech 20:427–438
30. Qian LF, Batra RC, Chen LM (2004) Static and dynamic deformations of thick functionally graded elastic plate by using higher-order shear and normal deformable plate theory and meshless local Petrov–Galerkin method. Composites Part B 35:685–697
31. Qian LF, Batra RC (2004) Transient thermoelastic deformations of a thick functionally graded plate. J Therm Stresses 27:705–740
32. Qian LF, Batra RC, Chen LM (2003) Free and forced vibrations of thick rectangular plates by using higher-order shear and normal deformable plate theory and meshless Petrov-Galerkin (MLPG) method. CMES: Comput Model Eng Sci 4:519–534
33. Qian LF, Batra RC, Chen LM (2004) Analysis of cylindrical bending thermoelastic deformations of functionally graded plates by a meshless local Petrov-Galerkin method. Comput Mech 33:263–273
34. Qian LF, Batra RC (2005) Design of bidirectional functionally graded plate for optimal natural frequencies. J Sound Vib 280:415–424
35. Qian LF, Batra RC (2005) Three-dimensional transient heat conduction in a functionally graded thick plate with a higher-order plate theory and a meshless local Petrov-Galerkin method. Comput Mech 35:214–226